Verification of the Integrity of Barriers Using Gas Diffusion

David B. Ward[1,3] and Cecelia V. Williams[2]

[1]SPECTRA Research Institute
2201 Buena Vista, S.E.
Suite 300
Albuquerque, NM 87102
(505) 243-2800

[2] Environmental Restoration Technologies Department
Sandia National Laboratories
P.O. Box 5800
Albuquerque, New Mexico 87185-0719
(505) 844-5722

Abstract

In-situ barrier materials and designs are being developed for containment of high risk contamination as an alternative to immediate removal or remediation. The intent of these designs is to prevent the movement of contaminants in either the liquid or vapor phase by long-term containment, essentially buying time until the contaminant depletes naturally or a remediation can be implemented. The integrity of the resultant soil-binder mixture is typically assessed by a number of destructive laboratory tests (leaching, compressive strength, mechanical stability with respect to wetting and freeze-thaw cycles) which as a group are used to infer the likelihood of favorable long-term performance of the barrier. Scaling up the laboratory methods to field situations presents serious technical challenges, such tests would render the waste form useless for its long-term purpose of waste isolation.

The need exists for a minimally intrusive yet quantifiable methods for assessment of a barrier's integrity after emplacement, and monitoring of the barrier's performance over its lifetime. A non-destructive test is needed that can be performed at both the laboratory and field scales, and

[3]Now at Jacobs Engineering Group, 2155 Louisiana NE, Suite 10000, Albuquerque, NM 87110,
 (505) 888-1300

that directly measures the properties of interest or is correlated with them. Here, we evaluate non-destructive measurements of inert-gas diffusion (specifically, SF_6) as an indicator of waste-form integrity. Low diffusivity is a desirable waste-form property because migration by diffusion is an important mechanism for contaminant loss, although the net loss rate is also influenced by dissolution and reprecipitation. Diffusion measurements using an inert gas provide conservative estimates of diffusivity under aqueous conditions. The goals of this project are to show that diffusivity can be measured in core samples of soil jet-grouted with Portland cement, validate the experimental method through measurements on samples, and to calculate aqueous diffusivities from a series of diffusion measurements.

This study shows that it is practical to measure SF_6 diffusion rates in the laboratory on samples of grout (Portland cement and soil) typical of what might be used in a barrier. This study has demonstrated the at the laboratory scale: (1) SF_6 is a nearly ideal tracer — inert with respect to most materials and readily detectable at trace levels (down to 5 ppb); (2) Diffusion of SF_6 into air may be as rapid as 0.073 cm^2/s, based on direct measurement; (2) Diffusion of SF_6 through the grout (Portland cement and soil) is on the order of 0.001–0.003 cm^2/s; and (4) Measurements of effective diffusion coefficient are reproducible to ± 10% or better. These results suggest that field-scale tests would also be feasible, and would provide a non-destructive method of evaluating the integrity of a barrier *in situ*. Diffusion of SF_6 through grout (Portland cement and soil) is at least an order of magnitude slower than through air. The use of this tracer should be sensitive to the presence of fractures, voids, or other discontinuities in the grout/soil structure. Field-scale measurements should be practical on time-scales of a few days.

Acknowledgments

Intentionally Left Blank

Contents

Tables

Figures

Symbols

A	cross-sectional area of the sample — L^2
A_{sp}	specific surface area of a porous material — L^2/M
C	concentration of SF_6 at a specific point — M/L^3
C_0	initial concentration of SF_6 in the supply reservoir — M/L^3
C_C	concentration of SF_6 in the collection reservoir — M/L^3
d	diameter of pressure-equalizing tube — L
D_0	bulk diffusion coefficient for SF_6 (e.g., in air or N_2) — L^2/T
D_S	effective diffusion coefficient for SF_6 in the sample — L^2/T
g	acceleration due to gravity — L/T^2
h	piezometric head — L
J	SF_6 flux (parallel to diffusion-cell or capillary axis) — $M/L^2/T$
k	permeability — L^2
K	hydraulic conductivity — L/T
L	length
L	length (thickness) of the sample (parallel to flow direction) — L
l_{pe}	length of pressure-equalizing capillary — L
M	mass
m	mass of SF_6 — M
Q	total flow rate — L^3/T
SF_6^M	Measured SF_6 concentration (M/M)
SF_6^*	Corrected SF_6 concentration (M/M)
SF_6^N	Normalized SF_6 concentration (M/M)
T	time
t	time — T
t_{lin}	time after which the linear approximation is valid — T
V_C	volume of collection reservoir — L^3
x	coordinate along diffusion-cell axis — L
ϕ	porosity — L^3/L^3
μ	dynamic viscosity — M/LT
θ	tortuosity — L/L
ρ	density — M/L^3
ρ_m	density of the non-porous solid; the matrix density — M/L^3

Introduction

In-situ barrier emplacement techniques and materials for the containment of high-risk contaminants in soils are currently being evaluated as an alternative to immediate removal or remediation. Because of their relatively high cost, the barriers are intended to be used in cases where the risk is too great to remove the contaminants, the contaminants are too difficult to remove with current technologies, or the potential for movement of the contaminants to the water table is so high that immediate action needs to be taken to reduce health risks. Consequently, barriers are primarily intended for use in high-risk sites where few viable alternatives exist to stop the movement of contaminants in the near term.

Under many circumstances, the most expedient and effective means of isolating contaminated soil from the environment is through *in situ* solidification to produce a single cohesive body. Such a waste form, called a barrier, should be mechanically strong and durable, and resistant to leaching of the incorporated waste constituents. Among the numerous solidification agents proposed for various sites, the most common ones are Portland cement, sulfur cement, bitumen, and polyethylene. More exotic binders include colloidal silica, Na-siloxane polymer and acrylic polymer (3M Co. cement restorer). The integrity of the resultant soil-binder mixture is typically assessed by a number of destructive laboratory tests (leaching, compressive strength, mechanical stability with respect to wetting and freeze-thaw cycles (cf. Franz *et al.*, 1994)), which as a group are used to infer the likelihood of favorable long-term performance of the barrier.

Assessing the integrity of the barrier once it is emplaced, and during its anticipated life, is a difficult but necessary requirement. Scaling laboratory methods to field situations presents serious technical challenges. Compressive strength, which serves as an indicator of mechanical durability in all of the laboratory tests, is most readily measured on small samples of uniform dimensions, but the measurements cannot be repeated because each sample is destroyed in the process. To apply compressive-strength testing at the field scale, the barrier would have to be exhumed and cored at a multitude of points to obtain a statistically valid sampling. Alternatively, the complete barrier could be subjected to some form of impact testing. In either case, such tests would render the waste form useless for its long-term purpose of waste isolation. Existing surface-based and borehole geophysical techniques, while providing a "picture" of the barrier, do not provide the degree of resolution required to assure the formation of an integral in-situ barrier.

A non-destructive test is needed that can be performed at both the laboratory and field scales, and that directly measures the properties of interest or is correlated with them. Here, we evaluate non-destructive measurements of inert-gas diffusion (specifically, SF_6) as an indicator of waste-form integrity. In the use of tracers for barrier verification it is important to understand how a tracer gas injected into the barrier volume will diffuse. For a tracer system to work, the tracer must 1) diffuse at significantly different rates through the barrier material compared with the surrounding medium so that breaches in the barrier will be readily detectable; 2) diffuse at a high enough rate such that monitors outside the barrier can be spaced at relatively large intervals from one another and still be able to detect the tracer in reasonable periods of time; and 3) diffuse at a

predictable rate given the soil characteristics. To determine if these diffusion assumptions are valid, a series of bench scale tests was performed.

Low diffusivity is a desirable waste-form property because migration by diffusion is an important mechanism for contaminant loss, although the net loss rate is also influenced by dissolution and reprecipitation. At the microscopic scale, diffusivity is a function of the connected porosity and a geometric factor, the tortuosity. At larger scales, additional factors must be considered, including the presence of voids and fractures, as well as heterogeneities due to incomplete mixing of the binder with the soil or due to the presence of waste components that could not be thoroughly homogenized (e.g., steel drums, contaminated lab ware). A comparison of diffusivities measured in the laboratory with those measured in the field would allow quantification of the influence of large-scale features and hence more realistic projections of waste-form performance. Diffusivity may also be correlated with other properties of interest, e.g., an inverse correlation with compressive strength might be expected, but such an investigation is beyond the scope of this project.

Diffusion measurements using an inert gas provide conservative estimates of diffusivity under aqueous conditions. Because gas diffusion measurements are performed on dry samples, the restrictive influence of swelling clays or other matrix materials is minimized, so diffusion is maximized. Aqueous diffusivities are easily calculated from gas-phase diffusivities by accounting for the differing mean free path of the molecules of interest.

The goals of this project are:

- Show that diffusivity can be measured in core samples of soil jet-grouted with Portland cement.

- Validate the experimental method through measurements on samples that have been characterized by other techniques and through measurements on artificial samples of known geometry.

- Calculate aqueous diffusivities from a series of diffusion measurements using a the semi-empirical *Kozeny-Carman* relationship.
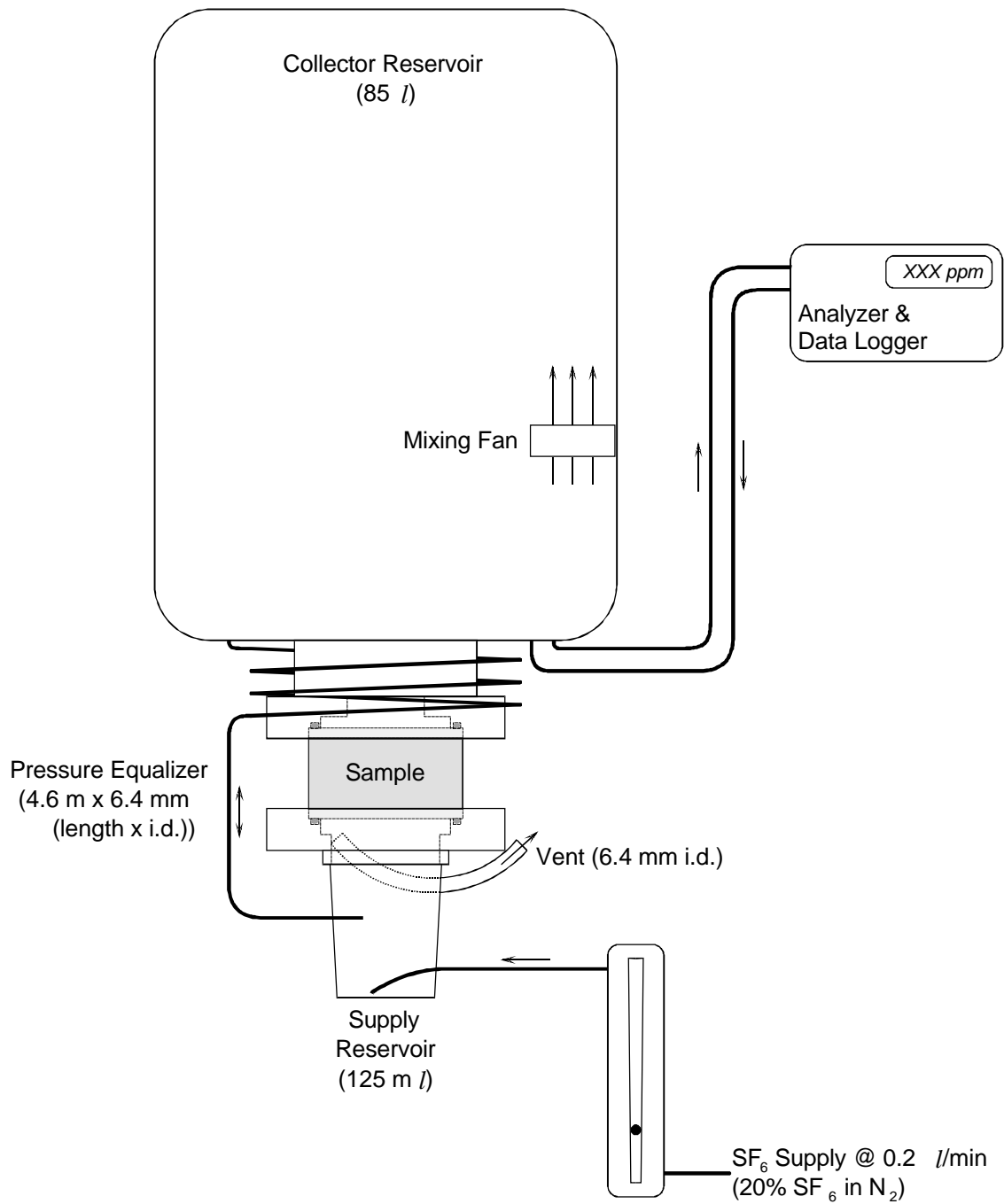
- Discuss application of this method to field settings.

Experimental Apparatus

In this study, diffusion coefficients for SF_6 were measured in the laboratory for cylindrical samples of jet-grouted mixtures of Portland cement and soil (see Heiser and Dwyer, 1995, for a description of the grouting method). The experimental setup was designed to permit one-dimensional diffusion only, parallel to the sample axis, Figure 1. The SF_6 concentration in the supply reservoir was maintained at a high constant value (~20% SF_6 in N_2), while the SF_6 concentration downstream of the sample was never more than ~300 ppm, which is negligible compared to the source concentration. Downstream concentration was monitored by a photo-acoustic IR gas analyzer (Bruel and Kjaer Model 1302, with filters for SF_6*), with a limit of detection of 5 ppb and a dynamic range of 10^5, giving an upper limit of measurement of ~500 ppm. Because 20% SF_6 has a specific gravity of 1.83 relative to air, the supply reservoir was located beneath the sample to eliminate the possibility of density-driven transport through the sample.

The epoxy-embedded core sample (see Methods section) was clamped between two machined plates with face-sealing O-rings, which in turn were open to the supply reservoir on one side and the collection reservoir on the other. The supply reservoir was constructed from a 125-m*l* wide-mouth polypropylene jar threaded into the sample holder. The inlet tube for SF_6 was located at the bottom of the jar, and a large (6.4 mm i.d.) vent tube was positioned near the surface of the sample. The SF_6 was introduced slowly (0.2 *l*/min) to minimize the pressure differential across the sample. A continuous flow of SF_6 was required in order to maintain a constant concentration in the supply reservoir because of the relatively high diffusivities of the samples, so this produced a continuous flow of SF_6 out the vent tube and precluded diffusion of ambient air into the supply reservoir.

The collection reservoir was made from a 75 *l* wide-mouth polypropylene carboy with a leak-proof seal. A mounting bushing passed through a 5 cm opening in the cap to mate with the sample holder and provide a gas-tight seal after caulking with silicone rubber. The minimum opening between the sample and the collection reservoir was 4.4 cm, providing good communication between the two regions. An electrical feed-through provided power for an 8.9 cm muffin fan, which ran continually to ensure that the reservoir was well mixed, avoiding ponding of the dense SF_6 at the bottom. The sampling and return lines for the gas-analyzer loop connected near the bottom of the reservoir.

* SF_6, CO_2, TCE and water.

Collector Reservoir
(85 l)

Mixing Fan

XXX ppm

Analyzer &
Data Logger

Pressure Equalizer
(4.6 m x 6.4 mm
(length x i.d.))

Sample

Vent (6.4 mm i.d.)

Supply
Reservoir
(125 m l)

SF_6 Supply @ 0.2 l/min
(20% SF_6 in N_2)

Figure 1. Diffusion cell.

A pressure-equalizing line connected the two reservoirs to ensure identical pressure in both, and hence zero pressure gradient across the sample. This line was 4.6 m long x 6.4 mm i.d., sufficient length so that diffusion was negligible during the measurement period. This was verified by calculating the rate of diffusion at steady-state. Beginning from Fick's first law of diffusion for steady-state conditions:

$$J = D_0 \frac{C_0}{l_{pe}} \;,$$ {1}

where J is the flux into the reservoir per unit cross-sectional area of the tube, D_0 is the diffusion coefficient, C_0 is the supply concentration (assumed to be constant at $2 \cdot 10^5$ ppm SF_6), and l_{pe} is the length of the pressure-equalizing tubing. The concentration gradient is thus C_0/l_{pe}, with the implicit assumption that the concentration in the collection reservoir is negligible in comparison to C_0. A tube of diameter d will have a cross-sectional area of $\rho d^2/4$, so the flux of mass m per unit time t into the reservoir will be:

$$\frac{dm}{dt} = J \frac{\rho d^2}{4} \;.$$ {2}

Dividing by the volume of the collection reservoir, V_C, gives:

$$\frac{1}{V_R} \cdot \frac{dm}{dt} = \frac{d\left(m/V_C\right)}{dt} = \frac{J \rho d^2}{4 V_R} \;.$$ {3}

The concentration in the collection reservoir (C_C) is mass per unit volume, corresponding to m/V_R here, and J may be expanded using Equation 1 to give:

$$\frac{dC_C}{dt} = \frac{D_0 C_0 \rho d^2}{4 \, l_{pe} V_C} \;,$$ {4}

which is the rate of change of concentration of SF_6 in the collection reservoir. The diffusion coefficient, D_0, is the only variable on the right-hand side that is not a function of the experimental setup. As a conservative proxy for D_0, the average diffusion coefficient for various gases into air was used (0.13 cm^2/s, Weast, 1973). Because of its size and mass, SF_6 must diffuse substantially more slowly. For a reservoir volume (V_C) of 85 l, tubing inside diameter (d) of 6.4 mm, and tubing length (l_{pe}) of 4.6 m, the calculated rate of increase of SF_6 in the collection reservoir is 0.013 ppm/min. This value is negligible in comparison to values from actual diffusion experiments (~5 ppm/min), and suggests that diffusion through the pressure-equalizing line may be safely ignored.

Less easily dismissed is the possible role of air pressure fluctuations driving SF_6 from the supply reservoir through the pressure-equalization tube to the collection reservoir. The experiments were performed in a laboratory located in a large modern four-story (+ basement) building with sealed windows and central heating and air conditioning. As the ventilation equipment cycled on and off, the building was pressurized and de-pressurized slightly. These pressure changes must have engendered some flow through the pressure-equalization line, lasting until equilibrium was

re-established. An increase in ambient pressure would have caused flow from the supply to the collection reservoir, resulting in a step-like increase in measured SF_6 concentration. A decrease in ambient pressure was less problematic, causing flow from the collection to the supply reservoir, resulting in a short-term dilution of the supply gas. This would have lasted only a few minutes until the supply reservoir was replenished by the continuous flow of SF_6. Much of the scatter observed in the measurements is probably attributable to such air pressure variations. Measurements made during weekends when the building ventilation was shut down were essentially noise-free.

Measurements were also made employing the alternate geometry for pressure equalization illustrated in Figure 2. Here, the pressure-equalization tubes from each reservoir were open to the ambient laboratory atmosphere. Calculations using Equation 4 show that SF_6 loss from the supply reservoir due to diffusion through the pressure-equalization tube was negligible at ~0.1%/h, and was two orders of magnitude less for the collection reservoir. To eliminate turbulence and any pressure differential, the SF_6 flow (0.2 l/min) into the sample reservoir was turned off after three minutes, and the vent was plugged. Thus the supply reservoir was completely static once it had been filled, so there was no gas motion across the supply-side of the sample. Additionally, fluctuations in ambient pressure could not have induced transport of SF_6 through the pressure-equalization lines because they no longer provided a direct link from the supply to the collection reservoirs. Changes in ambient pressure still played a role, however, because the two reservoirs probably did not equilibrate at the same rate, which led to transient pressure gradients across the sample. This in turn showed up as noise in the concentration profile versus time for the collection reservoir.
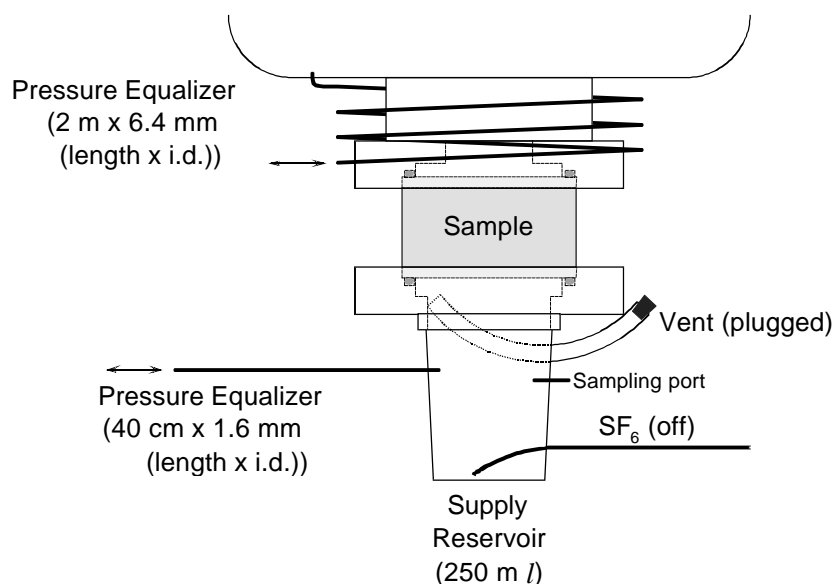
Figure 2. Alternate geometry for the diffusion cell.

Calculation of Diffusivity from Measurements

A series of measurements is initiated by filling the Supply Reservoir with SF_6 and then monitoring the SF_6 concentration in the Collection Reservoir as a function of time. After a transition period from zero diffusion to steady state, the rate of change of SF_6 concentration in the collection reservoir becomes essentially constant, and is a simple function of the geometry of the experimental apparatus, the diffusivity of the sample, and the concentration gradient. Beginning again with Fick's first law of diffusion for one dimension (along the x-direction, parallel to the diffusion-cell axis):

$$ J = -D_S \frac{dC}{dx} \quad . \tag{5} $$

Here, D_S is the effective diffusion coefficient of SF_6 in the sample. At steady-state, dC/dx will be uniform and constant throughout the sample and may be replaced with the macroscopic gradient measured across the whole sample:

$$ \frac{dC}{dx} = \frac{C_C - C_0}{L} \approx \frac{-C_0}{L} \quad , \text{ for } 0 < x < L . \tag{6} $$

Here, C_C and C_0 are the SF_6 concentrations in the collection and supply reservoirs, respectively, and L is the thickness of the sample. Experimental design ensures that $C_C << C_0$. However, the collection reservoir concentration C_C is the experimentally measured quantity. Its rate of change is related to the flux of SF_6 per unit time (dm/dt) as follows:

$$ \frac{dm}{dt} = J A = \frac{D_S C_0 A}{L} \quad , \tag{7} $$

where A is the cross-sectional area of the sample. Dividing both sides of Equation 7 by the collection-reservoir volume V_C gives the rate of concentration change, dC_C/dt:

$$ \frac{dC_C}{dt} = \frac{d(m/V_C)}{dt} = \frac{D_S C_0 A}{L V_C} \quad . \tag{8} $$

This is quantity extracted from the experimental measurements, once steady-state has been reached, by a linear regression of C_C versus t. The effective diffusivity of the sample is then found by solving Equation 8 for D_S.

The diffusion rate in the sample, D_S, can be related to the bulk diffusivity of SF_6 in air D_0, the porosity f, and tortuosity q (cf. Bear, 1972, p. 112):

$$ D_S = \frac{f \cdot D_0}{q^2} \quad . \tag{9} $$

15

Physically, the tortuosity may be thought of as the ratio of the actual path-length between two points in the sample to the straight-line distance between those two points. In practice, tortuosity is rarely measured directly, but is instead derived as a fitting parameter. When the porosity and bulk diffusivity are known from independent measurements, the tortuosity is easily calculated from Equation 9. If the porosity is unknown, then in principle both the porosity and tortuosity can be extracted from the time-dependent behavior of the concentration in the collection reservoir (Dykhuizen and Casey, 1989, and references therein).

At the beginning of a diffusion run, there is no SF_6 in the sample slab, and there is a significant delay until SF_6 diffuses through the sample and begins to accumulate in the collection reservoir. Thus, Equation 8 cannot be integrated realistically because the time- and position-varying concentration gradient within the sample initially violates the assumptions used in its derivation. A time-dependent description is well known, however (cf. Dykhuizen and Casey, 1989):

$$C_C(t) = \frac{AC_0}{V_C}\left[\frac{D_S t}{L} - \frac{f\,L}{6} - \frac{2f\,L}{p^2}\sum_{n=1}^{\infty}\frac{(-1)^n}{n^2}\exp\left(-\frac{D_S n^2 p^2 t}{f\,L^2}\right)\right] \quad . \qquad \{10\}$$

As time becomes large, the exponential term will disappear asymptotically. Thus,

$$C_C(t) = \frac{AC_0}{V_C}\left[\frac{D_S t}{L} - \frac{f\,L}{6}\right] \quad \text{for} \quad t \gg \frac{D_S p^2}{f\,L^2} \quad . \qquad \{11\}$$

The time-derivative of this equation is identical to Equation 8, which applies once steady-state has been reached. Furthermore, an estimate of the porosity may be obtained from Equation 11 by projecting the steady-state trend back to $t = 0$. This gives:

$$f = \frac{-6V_C\,C_C(0)}{ALC_0} \quad . \qquad \{12\}$$

Estimation of Hydraulic Conductivity from Diffusion Coefficients

Diffusion is the only mass-transport process at work under static conditions, but water in the subsurface is rarely static. Instead it flows through porous materials from regions of higher piezometric head to regions of lower piezometric head. This is expressed empirically in Darcy's Law. For a conduit of uniform cross-sectional area A and length L, the flow rate Q is given by

$$Q = KA\frac{h_1 - h_2}{L} \quad , \qquad \{13\}$$

where h_1 and h_2 are the initial and final piezometric heads, and K is the hydraulic conductivity. K has units of L/T. The hydraulic conductivity describes the intrinsic properties of the flow system, expressing the ease with which a fluid may flow, and is a function of both the fluid and the matrix. Mathematically, this is expressed as

$$K = k r g / m ,\qquad\qquad \{14\}$$

where k is the permeability of the matrix, r is the density of the fluid, g is the acceleration due to gravity, and m is the dynamic viscosity of the fluid. The permeability, with units of L^2, depends only upon the matrix and is independent of the properties of the fluid. Thus if permeabilities can be estimated from diffusion measurements, hydraulic conductivities can be calculated from Equation 14 and knowledge of the fluid properties.

A number of empirical relationships between permeability and various geometrical properties of porous media have been proposed (cf. Bear, 1972). These include terms such as *effective grain size* and various *shape factors*, and were derived to predict permeability in granular materials ranging from uniform spherical beads to poorly sorted angular sand grains. Applicability of such relationships to a non-granular matrix such as Portland cement is dubious at best, in part because it is unclear how the empirical fitting parameters should be measured in such a material.

The alternative is to proceed from a theoretical basis to arrive at a general expression for the permeability in terms of a few clearly defined physical properties. This has not been entirely achieved, but the *Kozeny-Carman equation* comes close, predicting permeabilities based on the surface area, porosity, tortuosity, and *Kozeny's constant*, which depends upon the geometry of the pores. Derivation of the *Kozeny-Carman equation* is outlined in Bear (1972). Briefly, the porous medium is considered to be a bundle of capillaries of equal length. Flow through a single capillary of circular cross-section is governed by Poisseuille's law, and non-circular cross-sections are accounted for by the introduction of a shape factor that can be calculated for simple geometries. The size of the capillaries leads to the concept of the hydraulic radius, defined as the ratio between cross-sectional area and wetted-perimeter length. The hydraulic radius is also measured by the ratio of porosity to surface area. By solving the Navier-Stokes equations for flow through all channels penetrating a cross-section normal to the flow direction, Kozeny was able to derive an expression for the permeability in terms of intrinsic matrix properties:

$$k = \frac{c_0 q f^3}{(1-f)^2 A_{sp} r_m} \quad .\qquad\qquad \{15\}$$

Here, c_0 is *Kozeny's constant*, A_{sp} is the specific surface area per unit mass, and r_m is the density of the non-porous solid matrix.

Carman's empirical studies showed that $c_0 q = \tfrac{1}{5}$ gave good agreement with experimental data, giving rise to the *Kozeny-Carman equation*:

$$k = \frac{f^3}{5(1-f)^2 A_{sp} r_m} \quad .\qquad\qquad \{16\}$$

Carman's experimental data was almost certainly obtained from measurements on *granular* porous media, so once again the question of applicability to Portland cement arises. It seems

17

likely that a cementitious material will have a much different pore geometry than a granular material, probably leading to $c_0 q \neq \frac{1}{5}$. A comparison of predicted and measured permeabilities may resolve this question.

Experimental Methods

Sample Preparation and Descriptions

A total of four core samples of jet-grouted Portland cement were obtained from the Landfill Demonstration Area in Tech Area 3 at Sandia National Laboratories. The grout was emplaced as part of a demonstration project, described in Allan and Kukacka (1994). Duplicate samples were obtained from two groutings ~75 cm in diameter by ~1 m high, which were part of an array of test groutings. The sample designated P36-1 was in place, but its exact location in the array is unknown because a pit only 1 m × 2 m was excavated. P36-2 was out of place, found at the edge of the excavation, but was known to have been located at the northeast corner of the array originally.

A detailed discussion of the composition of some of the test groutings is reported in Allan and Kukacka (1995). They report that the jet-grouted cement was a mixture of soil, cement, slag (in one test grouting), water, bentonite, and a "superplasticizer", giving a cementitious content of 16–26%. Soil in this area is a poorly-sorted sandy loam with occasional gravel-size rock fragments. The cured grout contains only faint flow-banding indicating nearly complete homogenization of the soil and cement. Allan and Kukacka report bulk densities ranging from 1.70 to 1.95.

The samples were cored *in-situ* from the test groutings using a hand-held industrial drill with a 10.16 cm (4 in) outside-diameter coring bit cooled with water. The extracted cores had a diameter of ~8.9 cm (3.5 in). The core samples were cleaned ultrasonically in deionized water for 20 min, rinsed in deionized water, and allowed to dry. Later, the ends were squared off with a water-cooled slab saw and then scrubbed with a brush under running tapwater and finally air-dried for at least one week before further treatment. When wet after each washing, the cores smelled strongly of Portland cement, suggesting that the grout may still be quite reactive chemically. The implications of this have not been investigated further.

The purpose of the various washing procedures was to remove all cutting debris that might otherwise reduce the permeability of the sample. The coring operation produced a lot of clay-size material which caked on the core surface. Ultrasonic cleaning removed most of this, but a good scrubbing would probably have been just as effective. The slab-saw cooling water also contained a lot of clay-size fines, but no caking occurred. The cores were scrubbed until no further loss of fines was evident visually, a process which required only a minute or so. Although deionized water was used for the ultrasonic wash, tapwater would have been adequate, as it was for later washing.

The cores were prepared for diffusion measurements. Casting in plastic (polyester resin [Plasticare Casting Resin] or epoxy resin [Shell Chemical Co. EPON 828 resin and Epi-Cure 3055 curing agent]). The encapsulated cores were sectioned using the slab saw to obtain a ~5 cm thick sample perpendicular to their axes. After sectioning, saw marks were polished out using a lap wheel with self-adhesive 120 grit SiC abrasive paper and tapwater.

Two casting methods were tested. In the first, an 11.43 cm (4.5 in) outside-diameter acrylic tube was used as a "consumable" form — it was left in-place after the resin cured, becoming an integral part of the sample holder. This proved troublesome. Polyester resin adhered strongly to the acrylic but only weakly to the sample. As the resin contracted upon curing, it pulled away from the core, opening a channel along the surface of the core. Epoxy resin formed a strong bond with the core but adhered only weakly to the acrylic tube, partially separating at this surface during sectioning and subsequent handling.

In the second casting method, a 12.06 cm (4.75 in) inside-diameter acrylic tube was used as a reusable form by coating its inside surface with a release agent (silicone high-vacuum grease for polyester resin, Miller-Stephenson TFE release agent for epoxy resin). This method worked well with both resins, but there appeared in places to be a thin film of air at the interface between the core and the polyester resin. As the film did not appear to be continuous, the sample (36-1a) was not recast. The epoxy formed a strong bond with the core and released easily from the form when the form was tapped with a soft mallet.

The epoxy-resin reusable-form casting method was superior. The epoxy exhibited negligible shrinkage, bonding well to the core, yet released easily from the mold using a clean easily applied release agent. It cured relatively slowly, however, and thus penetrated any fractures present. If the fractures connected with voids, these too became filled with epoxy. The epoxy did not appear to penetrate deeply into the grout itself, seeping only ~2 mm into the matrix from the edge of the core or any fracture surface. The curing reaction is exothermic, and can lead to significant temperature increases (maximum temperatures exceeding 100 °C in some cases) when casting large (>300 ml) volumes. To facilitate mixing, the resin was warmed to 60 °C before combining with the curing agent (at 25 °C), and had a pot-life of 20–30 min before heat generated by curing began to raise the temperature and accelerate the curing rate. This run-away condition did not occur once the epoxy was poured into the annulus surrounding the core sample in the casting form. Vacuum-degassing of the mixed epoxy was evaluated and found to be unnecessary. Only a few bubbles adhered to the sample or the walls of the form, while any suspended bubbles floated to the surface before curing was complete. The number of bubbles was not significantly reduced by ~15 min of degassing (longer degassing was not practical due to limited pot-life).

Polyester resin offers several advantages over epoxy if sample-adhesion could be improved. With the addition of the appropriate amount of catalyst, curing times can be much shorter, leading to much less penetration of fractures and voids. This would permit more realistic estimates of the bulk properties of the sample rather than focusing on the matrix. The polyester resin is also water-clear instead of dark translucent olive green. The casting process for either resin could be improved if the sample could be wrapped or coated with some material that would prevent impregnation but would not hamper adhesion. Another alternative might be to use an acrylic resin. Some acrylics cure very quickly (~5 min) and thus may not penetrate very deeply into fractures. They also exhibit low shrinkage. They are opaque, however, so quality of adhesion to the core would be difficult to verify visually, and open channels might not be detected until diffusion measurements were made.

Individual samples are summarized in Table 1. The suffixes a and b distinguish among duplicate samples from the same test grouting. Dimensions of the prepared samples were measured using digital calipers. The quoted diameter is an average value of the minimum and maximum diameters of the top and bottom surfaces, and the range is the difference between the smallest and largest measured diameters. The quoted height is an average of the minimum and maximum heights, and the range is the difference between the minimum and maximum heights. Void space and clast fractions on the top and bottom surfaces were estimated visually (top and bottom are with respect to the orientations of the cores as sampled from the Chemical Waste Landfill Demonstration Area).

Table 1. Sample descriptions.

| Sample	Casting Method	Dimensions (mm); Top, Bottom (%)		Comments
36-1a	Resin: Polyester Form: Removable	Diameter: Range: Height: Range: Voids: <1%, 2% Clasts: 10%, 15%	94.5 ±0.1 51.2 ±0.9	Slight separation of the resin from the core near the top and bottom, possible connected pathway from top to bottom. One void on the bottom extends several centimeters into the sample.
36-1b	Resin: Epoxy Form: Integral	Diameter: Range: Height: Range: Voids: 2%, 2% Clasts: 3%, 10%	94.4 ±0.1 50.8 ±0.6	Partial separation at acrylic/epoxy interface, but no connected pathway from top to bottom, and this area is outside of seal so will not see SF_6. Six hairline fractures are visible on the top surface; only three on the bottom. A large clast (3 cm x 2 cm) is exposed on the bottom.
36-2a	Resin: Epoxy Form: Removable	Diameter: Range: Height: Range: Voids: 7%, 7% Clasts: 3%, 5%	94.6 ±0.2 47.8 ±0.7	Was first cast using polyester resin, but adhesion was poor so old resin was chipped off. Voids are numerous and small (usually < 3 mm). Soil clots were not counted as clasts, as their porosity is high. Few were present on the top, but they constituted ~3% of the bottom. Several small fractures oriented radially from the edges are filled with epoxy, but there is no general impregnation.
36-2b	Resin: Epoxy Form: Removable	Diameter: Range: Height: Range: Voids: 5%, 4% Clasts: 7%, 4%	94.4 ±0.6 46.2 ±1.2	Contains a fracture parallel to the axis of the core. The fracture and several large voids became filled by epoxy during casting, and were counted as clasts.

In the following images of the top and bottom surfaces of each prepared core sample (Figures 3–6), large voids are overlaid with a "V", and smaller voids (> 0.5 mm) are indicated by lines connecting them to a "V". Dark clasts without labels are rock fragments. Lighter clasts labeled "S" are clots of indurated soil. In several places, the epoxy seeped along fractures and filled adjoining voids. These features have been labeled with "E".

The top and bottom surfaces of P36-1a are shown in the images in Figure 3. Rock fragments are abundant, and are predominantly feldspar, quartz, and fine-grained metamorphic rocks derived from weathering of the nearby Manzano Mountains. These lithologies have little porosity and will act as barriers to diffusion. Two lighter-colored clasts labeled "C" are also present on the top surface, and appear to be fragments of Portland cement; one of these contains small rock fragments of the same lithology as described above. There are only a few shallow voids on the top surface, but two large voids on the bottom significantly penetrate the sample. The void at 1 o'clock is 2 cm deep and extends laterally beneath the surface for 1 cm towards the axis of the sample. The other large void, at 3 o'clock, is approximately 1 cm deep and no wider than where it intersects the surface. Linear features visible on both surfaces are artifacts of the polishing process. Slight flow-banding may be discerned on the top surface. This sample was cast in polyester resin using the removable form. The resin separated slightly from the core near the top and bottom, as evidenced by a reflective film of air between the resin and the core which indicated that a connected pathway may extend from top to bottom over ~25% of the circumference.

As may be seen in Figure 4, P36-1b differs slightly from P36-1a, containing fewer rock fragments but slightly more medium-size voids (<5 mm). Larger voids are also present on each surface, significantly penetrating the sample up to 1 cm. A large clast (3 cm x 2 cm) is exposed on the bottom. The most critical difference may be the network of hairline fractures evident on the top and bottom surfaces, which may provide low-tortuosity paths for SF_6 diffusion. Linear features visible on both surfaces are artifacts of the polishing process. This sample was cast in epoxy using an integral acrylic form. Partial separation occurred at the acrylic/epoxy interface, but no connected pathway extends from top to bottom, and this area is outside of the seal so will not be subjected to SF_6.

The top and bottom surfaces of P36-2a are shown in Figure 5. The cement matrix is gray rather than nearly white as it is in the P36-1 samples. Rock fragments are not very numerous, but there are several clots of indurated sand, labeled with "S". Although there are no large voids on the top surface, there are numerous smaller ones, most of which penetrate beyond visual range (>3–5 mm). The bottom surface is even more riddled with voids, and contains several large ones, ~1 cm across. Some of these appear to be cavities remaining from sand clots that were disaggregated and washed away during cutting and washing. A fracture on the bottom surface at 5 o'clock penetrates several centimeters into the sample and was filled with epoxy during casting, as were several other smaller fractures visible around the edges of this surface. There is no general impregnation of the sample by the epoxy. This sample was first cast using polyester resin, but adhesion was poor so the resin was chipped off, and the sample was recast using epoxy and the removable form. The epoxy bonded well to the sample surface, leaving no air channels.

As may be seen in Figure 6, the cement matrix of P36-2b is very similar to that of P36-2a in terms of the distribution of small voids, rock fragments, and soil clots. The distinguishing feature of this sample is a fracture and several associated voids that cuts across the top surface. During casting, epoxy seeped along this fracture and filled the adjoining voids, but did not impregnate the cement matrix. On the bottom surface, this fracture only penetrates halfway across the sample. The plane of the fracture appears to be approximately parallel to the axis of the sample. This sample was cast in epoxy using the removable form; the epoxy bonded well to the sample surface, leaving no air channels.
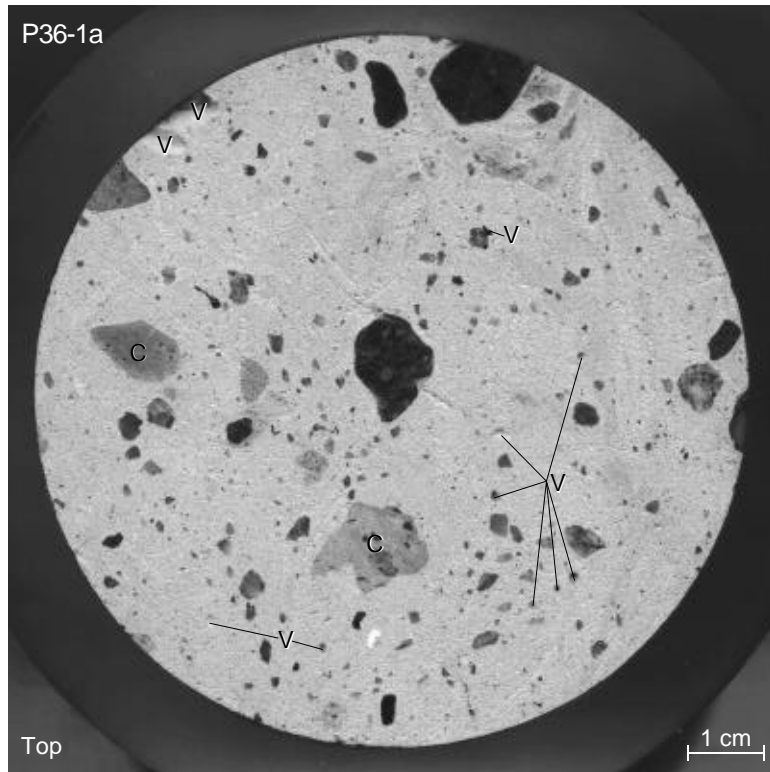
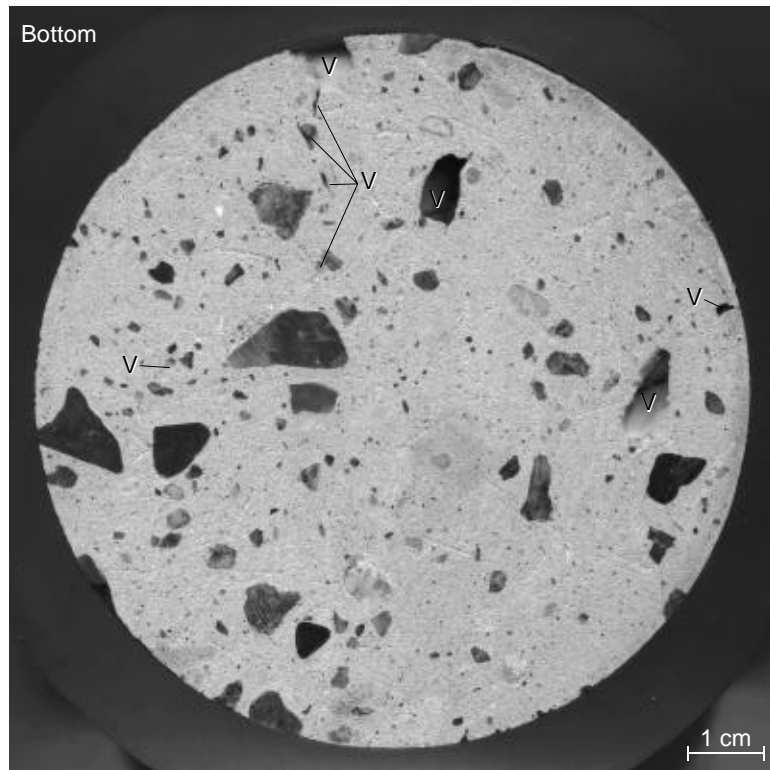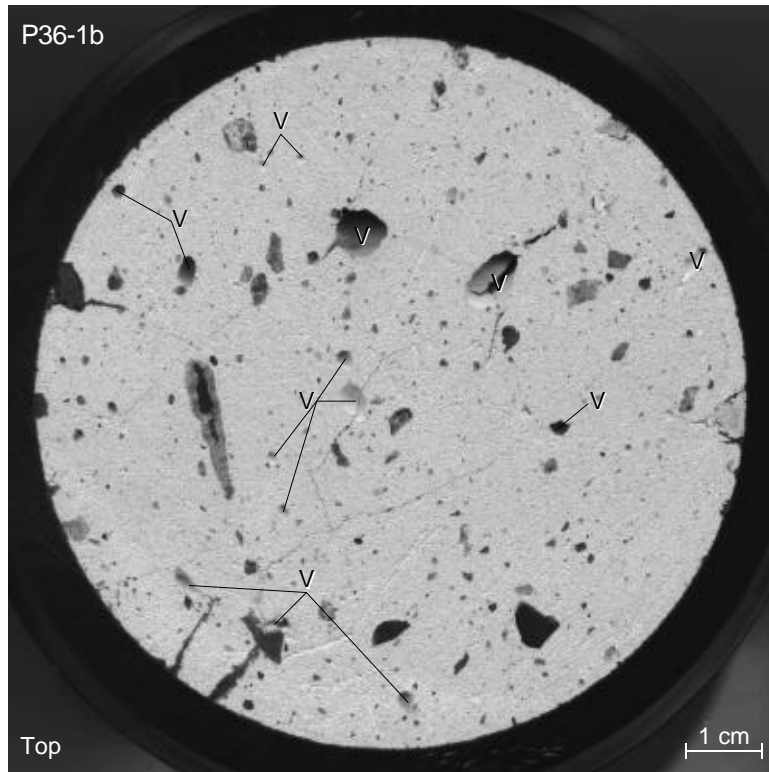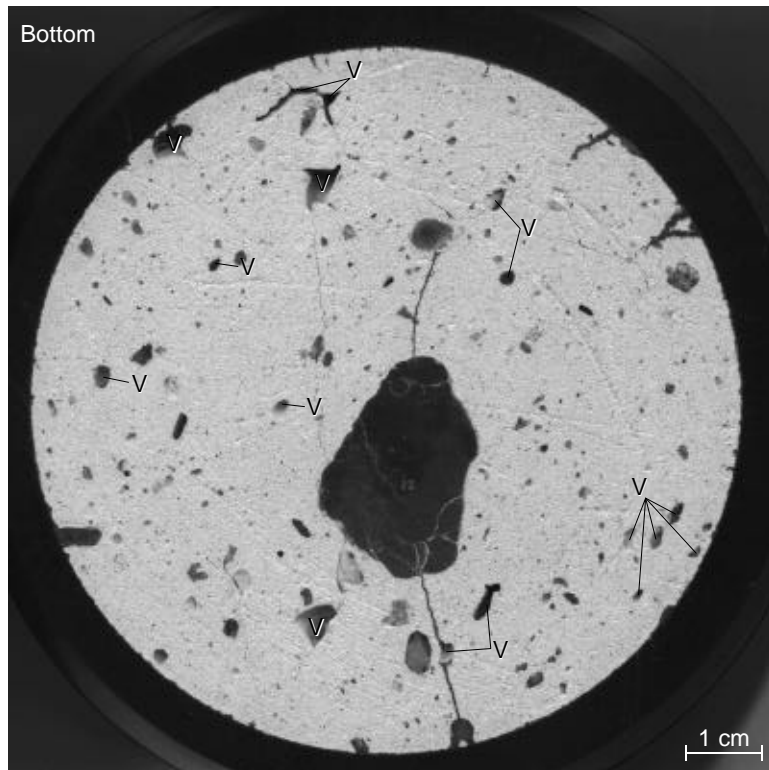**Figure 3. P36-1a top and bottom surfaces.**
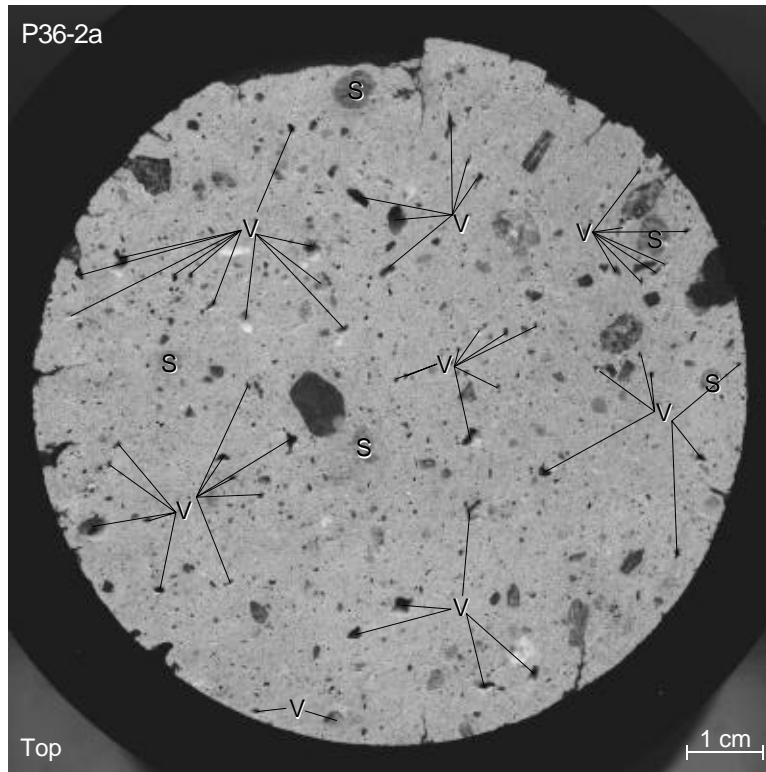
P36-1b

Top

1 cm

FOLD

Bottom
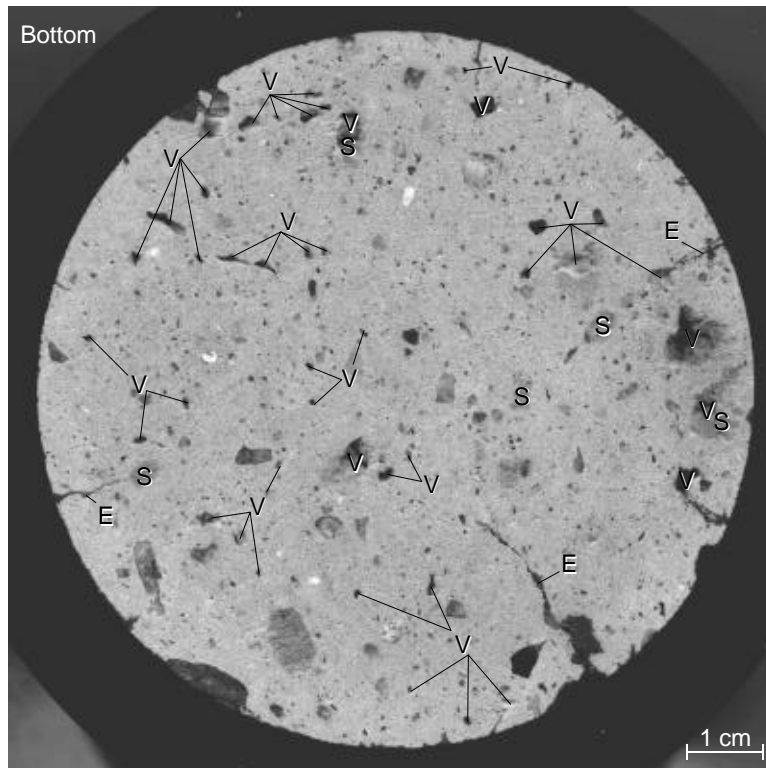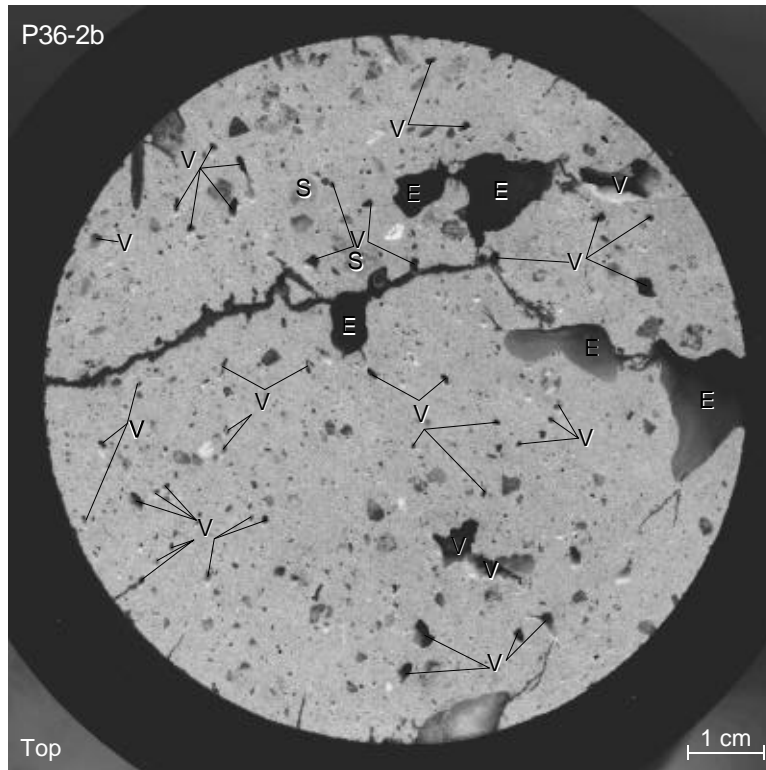
1 cm

Figure 4. P36-1b top and bottom surfaces.
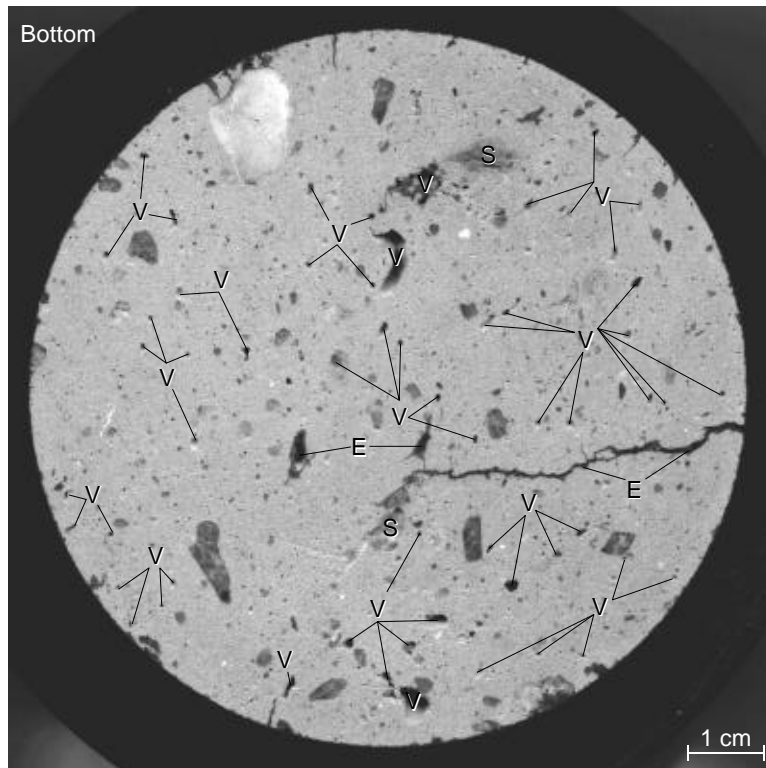
Figure 5. P36-2a top and bottom surfaces.

Figure 6. P36-2b top and bottom surfaces.

Surface Area Determinations

All surface areas were measured by N_2-BET using a fully automated Micromeritics ASAP 2000 following standard methods. The end pieces that were cut from each core sample were lightly crushed, and a few grams of chips (≤ 5 mm in longest dimension) were hand-picked for surface-area analysis, avoiding clasts. Samples were degassed overnight (15–23 h) at 50°C before analysis. Higher temperatures would have risked excessive loss of water from the cement gel (cf. Lea, 1971) Replicate analyses differed by less than 1%, even after an additional 7 h of degassing.

Diffusion Measurement Protocol

Instrument Operation

The Bruel and Kjaer Model 1302 photo-acoustic gas analyzer was configured with the following filters in addition to the standard water vapor filter (gas and detection limits in parentheses): UA 0936 (SF_6 0.7 ppm), UA 0978 (trichloroethylene), UA 0983 (CO_2 1.7 ppm), and UA 0988 (SF_6 0.005 ppm). Measurements for SF_6 were performed using UA 0988 with interference corrections for trichloroethylene, CO_2, and water vapor. An MS-DOS personal computer was used as a data logger, running the software supplied with the instrument and connected to the gas analyzer via RS-232C serial ports. The instrument was configured using parameters of 626 mm Hg for the local air pressure (a typical value for Albuquerque), a temperature of 22.5°C, and an inlet tube length of 1.92 m (1.68 m of 3.175 mm i.d. tubing was used, whereas the instrument was calibrated for 3 mm i.d. tubing). The instrument was allowed to warm up by taking continuous readings for at least 20 minutes before any measurements on samples or standards were made. The instrument was configured to measure continuously, with no delay between samples. Measurements were logged by attached computer and data reduction was performed later.

The gas analyzer was leased from Bruel and Kjaer in a fully calibrated condition. Calibration was verified by running a 259 ppm SF_6 standard in N_2 before each measurement run, and the difference between the measured value and the nominal value was used as a normalizing factor to correct measurements on unknowns. Except for a two-day period of erratic behavior, readings were quite stable, with measured values for the 259 ppm standard ranging from 209 to 211 ppm over a 14 day period. The difference between the nominal value and the measured values was due to declining sensitivity near the upper end of the instrument's measurement range. A calibration curve accounting for this was developed.

The standard gas was measured using two different methods. In the first, recommended by Bruel and Kjaer, SF_6 was vented through an open-ended line at 2 *l*/min. A tee 1 m from the end branched to the gas analyzer, and a flow gauge downstream of the tee verified that positive flow was maintained during sampling. In the second, a Tedlar gas-sampling bag was first evacuated using a 60 m*l* syringe, and then was filled with ~1 *l* of the standard gas. For analysis, the gas analyzer was connected directly to the bag. Results of the two methods were indistinguishable.

Measurement of Samples Requiring Dilution

The concentration of the supply-reservoir gas (~20% SF_6) could not be measured directly using the UA 0988 filter, but required a 1:1000 dilution. Also, development of a calibration curve required a series of dilution of the 259 ppm standard gas. Dilutions were performed volumetrically using a set of syringes with nominal volumes of 1, 5,10, 60, and 1000 ml. Actual volumes were determined gravimetrically using water, and were precise to 0.005 ml or 0.1%, whichever was larger. Compressed air from the building's physical plant was used as the diluent. The requisite volumes were mixed in a Tedlar gas-sampling bag that had first been evacuated by hand using a 60-ml syringe. Dilutions of the 259 ppm standard mixed readily with air, yielding consistent readings after gentle agitation. Dilutions of the 20% SF_6 required more severe mixing — after both SF_6 and air were injected into a Tedlar bag, an empty 60-ml syringe was attached and rapidly cycled ten times. To reduce errors, all syringes were first "rinsed" several times with the gas they were to be filled with before measuring the actual aliquots. For analysis, the gas analyzer was connected directly to the bag.

Sample Diffusion Measurement

A series of measurements on a sample in the diffusion cell began with several minutes of monitoring to establish an accurate baseline before 20% SF_6 was introduced into the supply reservoir (the baseline was often greater than zero because of residual SF_6 from previous runs). After the baseline was established, the time was noted and the SF_6 flow was started at a rate of 0.2 l/min, which was maintained throughout the measurement series (method 1, geometry as in Figure 1), or was shut off after three minutes (method 2, alternate geometry as in Figure 2). In method 2, a sample of the supply reservoir was taken two minutes after the SF_6 was shut off. Monitoring continued until the SF_6 concentration in the collection reservoir reached ~200 ppm. Then the supply reservoir was sampled and diluted in duplicate and measured. Finally, one or more aliquots of the 259 ppm standard were measured.

The time associated with each measurement must be corrected for the time lag inherent in the system. The two most important lags are the time required to fill the supply reservoir, and the time required to mix the collection reservoir. These are accounted for by a single offset, which was determined from a series of measurements on a solid disk with an orifice of ~8 mm dia. × ~27 mm long. Regression of concentration vs. time yielded a time-intercept of 92 s for the 125 ml reservoir (method 1) or 134 s for the 250 ml reservoir (method 2).

Results

Measurements were made to determine a calibration curve for the gas analyzer, to constrain possible values of the bulk diffusion constant for SF_6 into air, and to determine diffusion coefficients for SF_6 through jet-grouted Portland cement. Surface area measurements were made so that the diffusion coefficient could be related to hydraulic properties.

Surface Area Measurements

Surface area (A_{sp}) measurements by N_2-BET are listed in Table 2. Accuracy of the measurements may be estimated from deviation between nominal and measured values for the 10.9 m^2/g standard, which amounts to ~3%. Variation from sample to sample from the same grouting exceeds the variation between the two groutings. The cause of these variations is probably due to small sample size and lack of representativeness, and they indicate that extrapolations from measurements on a few chips to an entire cored sample may have an additional uncertainty of 6–8%.

Table 2. Surface areas by N_2-BET.

Sample	A_{sp} (m^2/g)
P36-1a	23.41
P36-1b	27.34
P36-2a	23.46
P36-2b	20.41
Standard (10.9 m^2/g)	10.62

Calibration Curve

Although the Bruel and Kjaer gas analyzer has a dynamic range of five orders of magnitude, from 0.005 to 500 ppm, the upper two decades of this range exhibit a significant and progressive fall-off in sensitivity. To compensate for this, a calibration function was fit to a set of measurements on dilutions of the standard gas, ranging in concentration from 0.266 to 259 ppm, as shown in Figure 7. The calibration function was optimized by minimizing the sum of residual^2/(actual value)^2 calculated for each point. Several functional forms were examined as well. At low concentrations, the measured values exceeded the actual values, suggesting that some component of the calibration function must be less than zero at low concentrations. This was achieved by including the logarithmic term, resulting in the following function:

$$SF_6^* = (1.6993E-6)(SF_6^M)^{3.05475} + (SF_6^M)\left(0.94485 + (2.3861E-4)\ln(SF_6^M)^4\right), \qquad \{17\}$$

where SF_6^M is the measured value and SF_6^* is the corrected value. Except for the logarithmic term, all terms are monotonically increasing, so the function can have at most one inflection point. Because this function cannot change direction to pass through each point, but instead must be a smooth curve, the magnitude of the residuals provides an estimate of the analytical precision of the measurements. Between 2 and 260 ppm, the residuals average less than $\pm\,0.23\%$ of the measured values, suggesting that this aspect of the measurement process in an insignificant source of uncertainty.

After correcting for non-linear response, measurements were normalized according to a concurrent measurement on the 259 ppm SF_6 standard, $SF_6^*(259)$. This may be expressed mathematically as:

$$SF_6^N = SF_6^* \cdot \frac{259}{SF_6^*(259)} \quad . \tag{18}$$

Because of the stability of the gas analyzer, this final correction amounted to less than 0.5% in all cases.
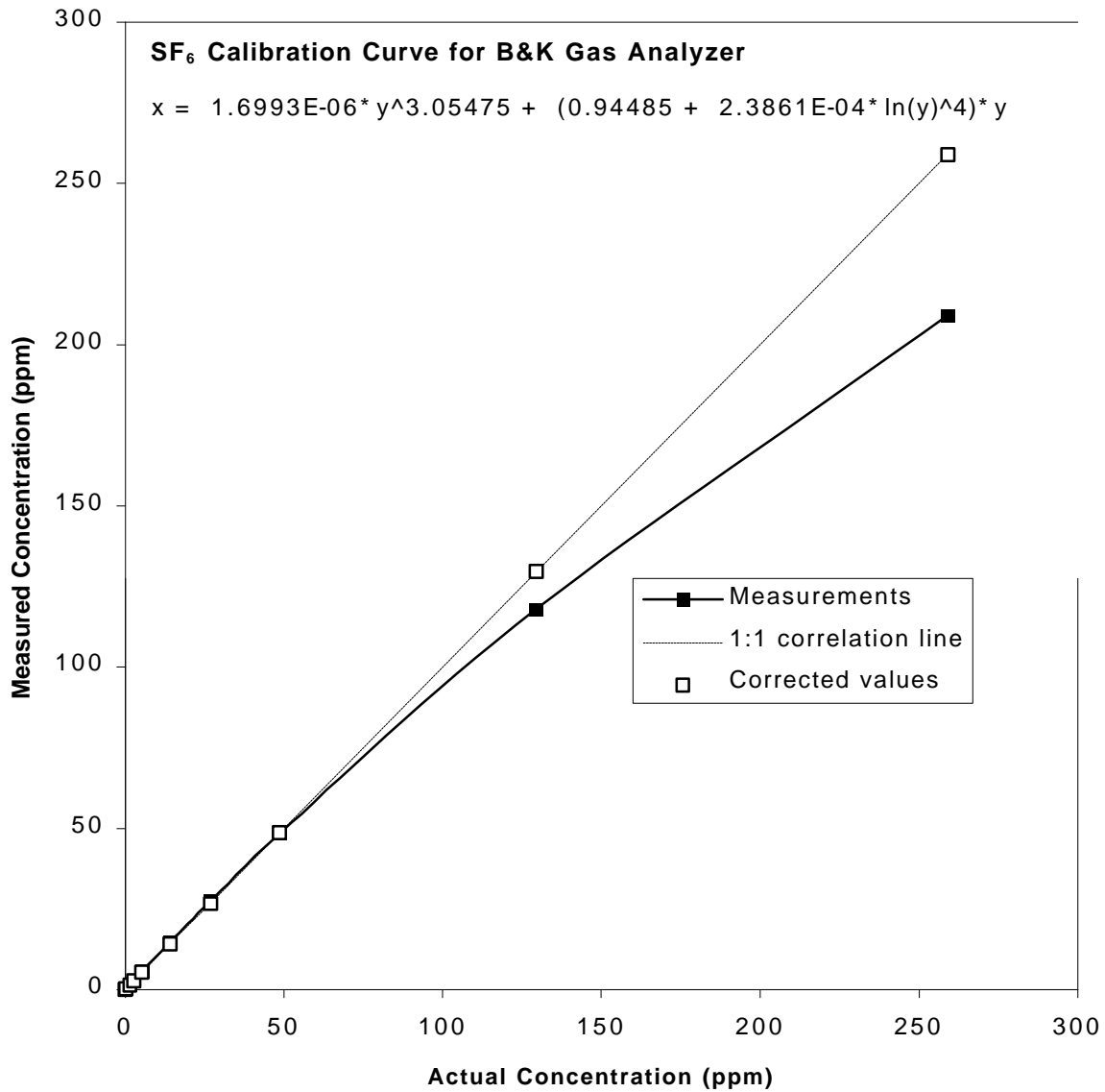
Figure 7. Calibration curve for gas analyzer.

Measurement of the SF$_6$ Diffusion Coefficient into Air

The bulk diffusion coefficient of SF$_6$ into air (D_0) was measured by using an orifice of known dimensions in place of the sample. The alternate diffusion-cell geometry was used (Figure 2 on p.14) in which the pressure in each reservoir was equalized with the ambient pressure through tubes open to the laboratory atmosphere.

Collection-reservoir profiles for two different orifices are shown in Figures 8 and 9. The concentration jump between 0 and 5 minutes illustrates the effect of the slight pressure differential present when SF$_6$ was flowing into the supply reservoir. Slight irregularities in the trend of the data at later times was probably due to fluctuations in ambient pressure in the laboratory as the building ventilation system switched on and off. The supply reservoir was sampled at 5 min and

at the end of the run, and changed from 16.8% to 13.8% (Orifice A) or 16.3% to 14.1% (Orifice B). The average value is shown on the figures and was used in subsequent calculations, along with an analytical precision estimated from replicate analyses on the supply gas.

The bulk diffusion coefficient, D_0, is a simple function of the experimental geometry and the slope of the concentration profile, as given by Equation 4 on p. 13. Rearranging this equation to solve for D_0 gives:

$$D_0 = \frac{4\,l_{pe}V_C}{C_0 \rho d^2} \cdot \frac{dC_C}{dt} \; . \qquad \{19\}$$

Errors were calculated assuming that C_0 and the slope were the only significant sources of uncertainty, and thus represent the internal precision of the measurement procedure.
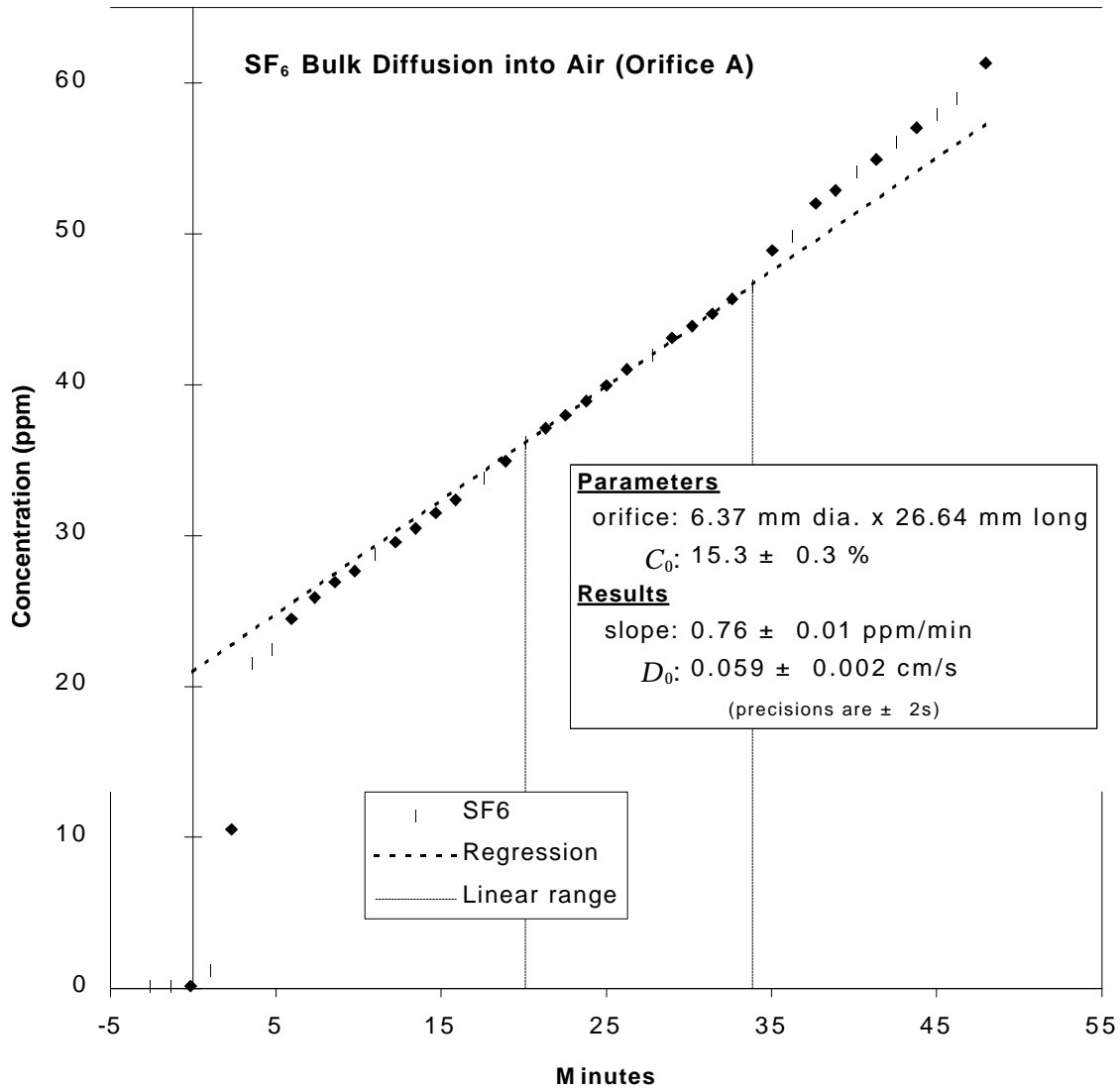
Figure 8. SF$_6$ bulk diffusion into air (orifice A).
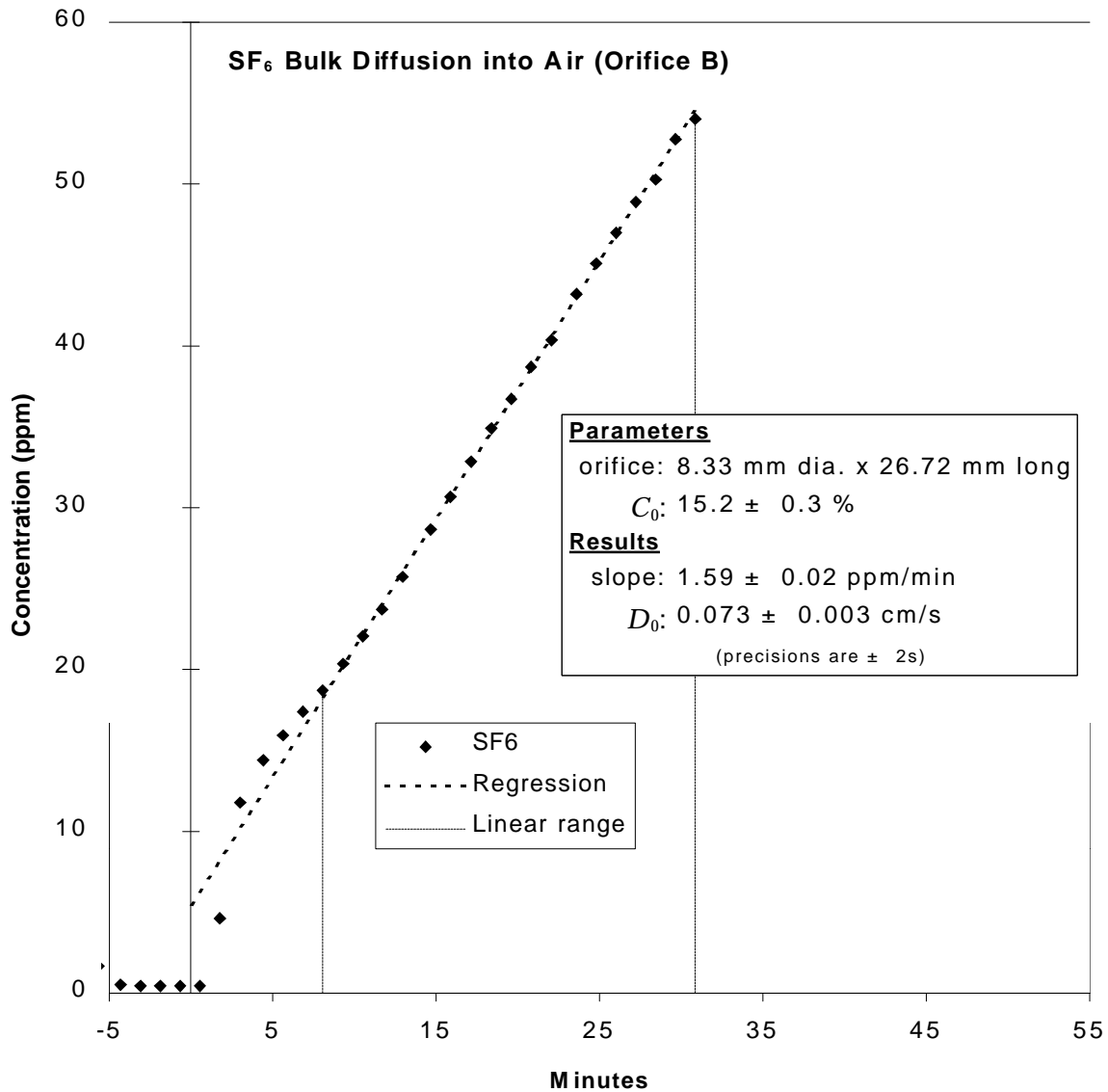
Figure 9. SF$_6$ bulk diffusion into air (orifice B).

Measurements on Core Samples

Diffusion profiles for the four core samples of jet-grouted Portland cement (P36-1a, P36-1b, P36-2a, and P36-2b) are presented in Figures 10–13. Two measurement geometries were used, designated methods 1 and 2. In method 1, the diffusion cell was configured as shown in Figure 1 on p.12, with a pressure equalization line connecting the supply and collection reservoirs. During these measurements, SF$_6$ flow to the supply reservoir was maintained at a constant 0.2 *l*/min, ensuring a constant SF$_6$ concentration in the supply reservoir. In method 2, the diffusion cell was configured as shown in Figure 2 on p.14. A perceptible shallowing of the diffusion profiles at late times for this method is evident in Figures 10 and 11, caused by a slow decrease in the concentration of SF$_6$ in the supply reservoir over the course of a run.

34

In principle, the two methods should be equivalent because neither should permit the existence of a pressure gradient across the sample. In practice, method 1 always gave a steeper slope, implying the existence of a slight pressure gradient or some effect related to the continual movement of gas across the supply-side face of the sample in method 1. The difference is greater than can be explained by differences in supply-reservoir concentrations. Both methods were sensitive to variations in ambient pressure. During periods when the building ventilation system was cycling every few minutes, the measured profile became somewhat scattered and significantly steeper, as may be seen in Figure 12. Here, the method 1 profile is noisy and much steeper relative to the method 2 profile than was observed for any of the other three samples.

In method 1, the supply reservoir concentration was determined at the by sampling at the end of each run. In method 2, the supply reservoir was sampled at 5 minutes and at the end of the run, permitting the rate of decrease to be calculated. Diffusion through a sample required a significant amount of time, however, so the time lag was taken to be the time elapsed from introduction of SF_6 (already corrected for the time lag of filling the supply reservoir) to the point of steady-state behavior. Thus the effective value for C_0 was not its value at the midpoint of the linear interval, but instead was its value 15–20 minutes earlier.
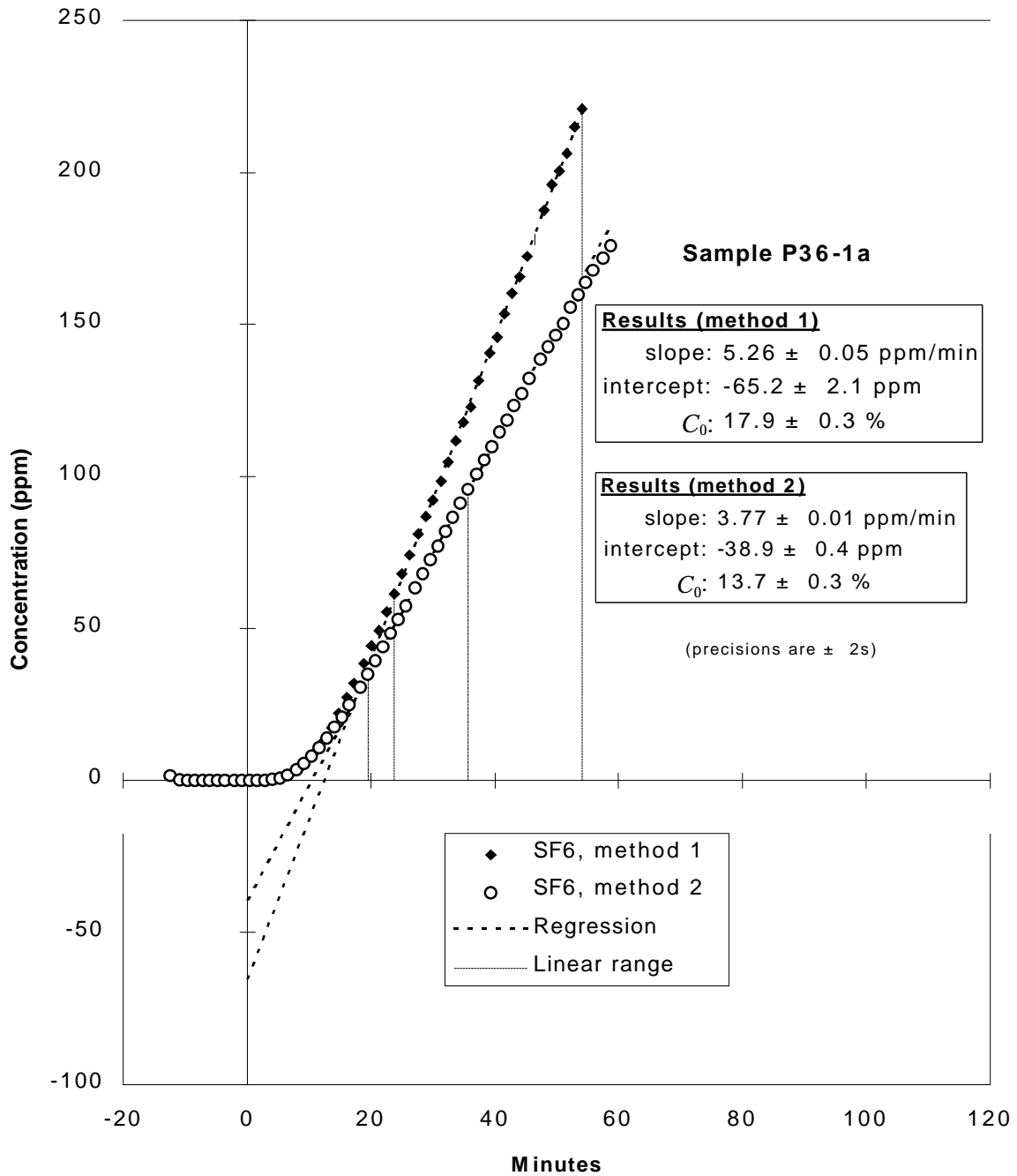
Figure 10. SF$_6$ diffusion profile for P36-1a.

The following text labels appear within the figure:

Concentration (ppm)

250

200

150

100

50

0

-50

-100

Sample P36-1a

Results (method 1)
slope: 5.26 ± 0.05 ppm/min
intercept: -65.2 ± 2.1 ppm
C_0: 17.9 ± 0.3 %

Results (method 2)
slope: 3.77 ± 0.01 ppm/min
intercept: -38.9 ± 0.4 ppm
C_0: 13.7 ± 0.3 %

(precisions are ± 2s)

SF6, method 1
SF6, method 2
Regression
Linear range

-20   0   20   40   60   80   100   120

Minutes
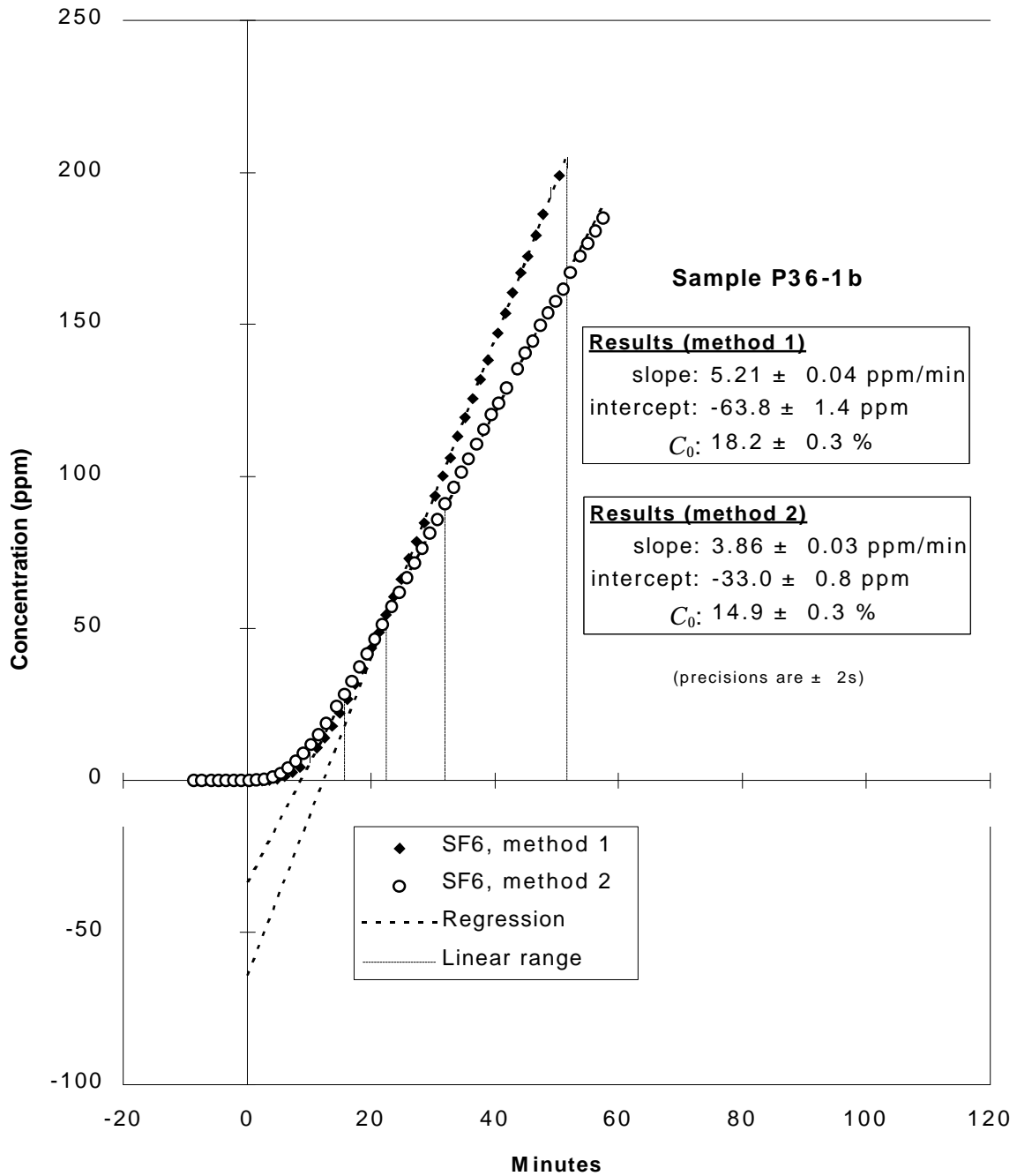
Figure 11. SF$_6$ diffusion profile for P36-1b.
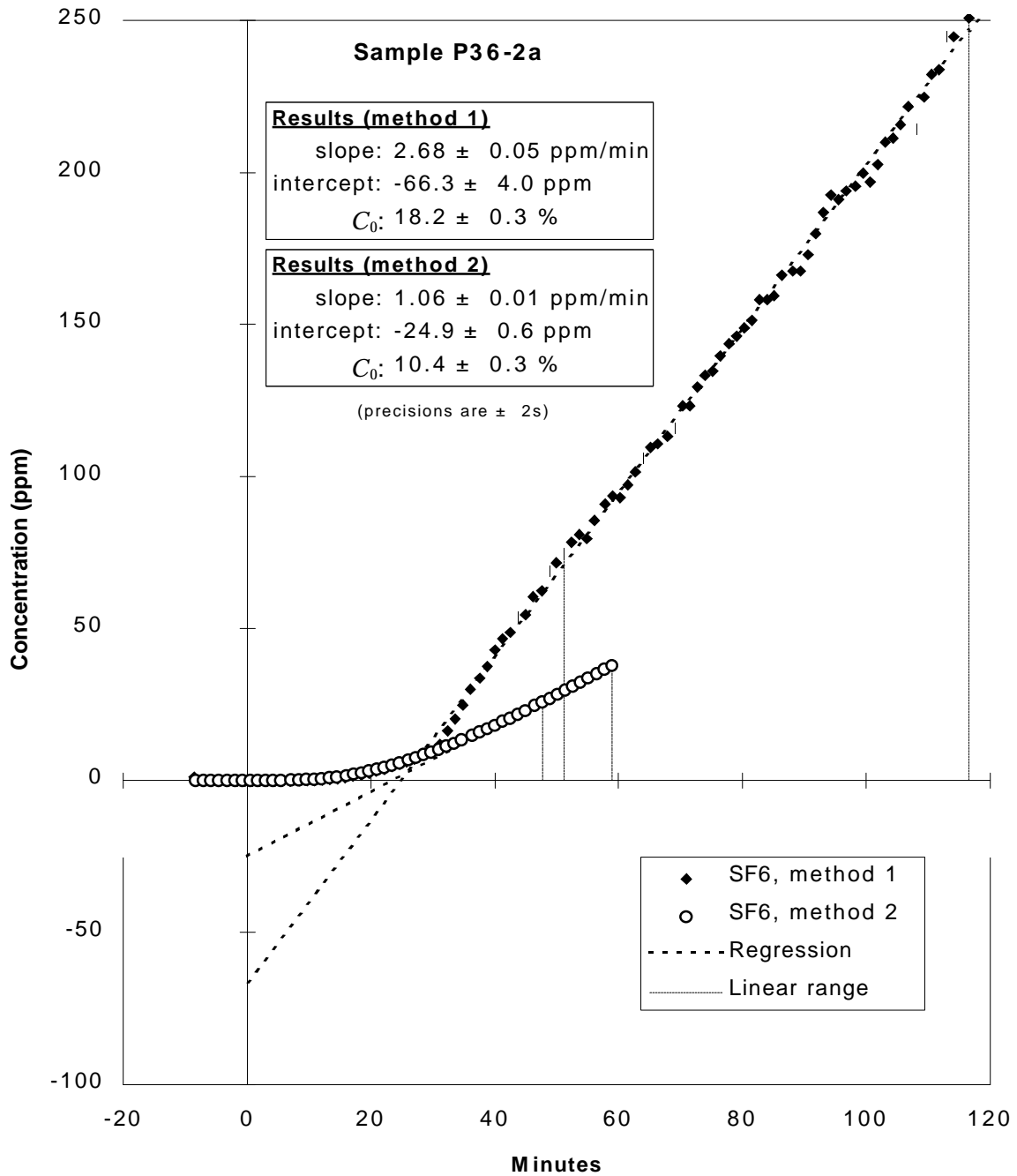
Figure 12. SF₆ diffusion profile for P36-2a.

The figure is a scatter plot titled "Sample P36-2a" with the y-axis labeled "Concentration (ppm)" ranging from -100 to 250, and the x-axis labeled "Minutes" ranging from -20 to 120.

Results (method 1)
slope: 2.68 ± 0.05 ppm/min
intercept: -66.3 ± 4.0 ppm
C_0: 18.2 ± 0.3 %

Results (method 2)
slope: 1.06 ± 0.01 ppm/min
intercept: -24.9 ± 0.6 ppm
C_0: 10.4 ± 0.3 %

(precisions are ± 2s)

Legend:
- SF6, method 1
- SF6, method 2
- Regression
- Linear range

Figure 13. SF$_6$ diffusion profile for P36-2b.

Discussion

Bulk Diffusion Coefficient for SF_6 Self-Diffusion

Before the expected time-dependent behavior of the diffusion measurements can be calculated, an estimate of the bulk diffusion rate of SF_6 (D_0) is needed. Stefanov *et al.* (1991) report a value for the self-diffusion rate of SF_6 calculated from their best-fit equation-of-state based on an exhaustive review of the available experiments. Their value is $\rho D_0 = 1.933 \times 10^{-5}$ kg/m·s (interpolated) at $25°C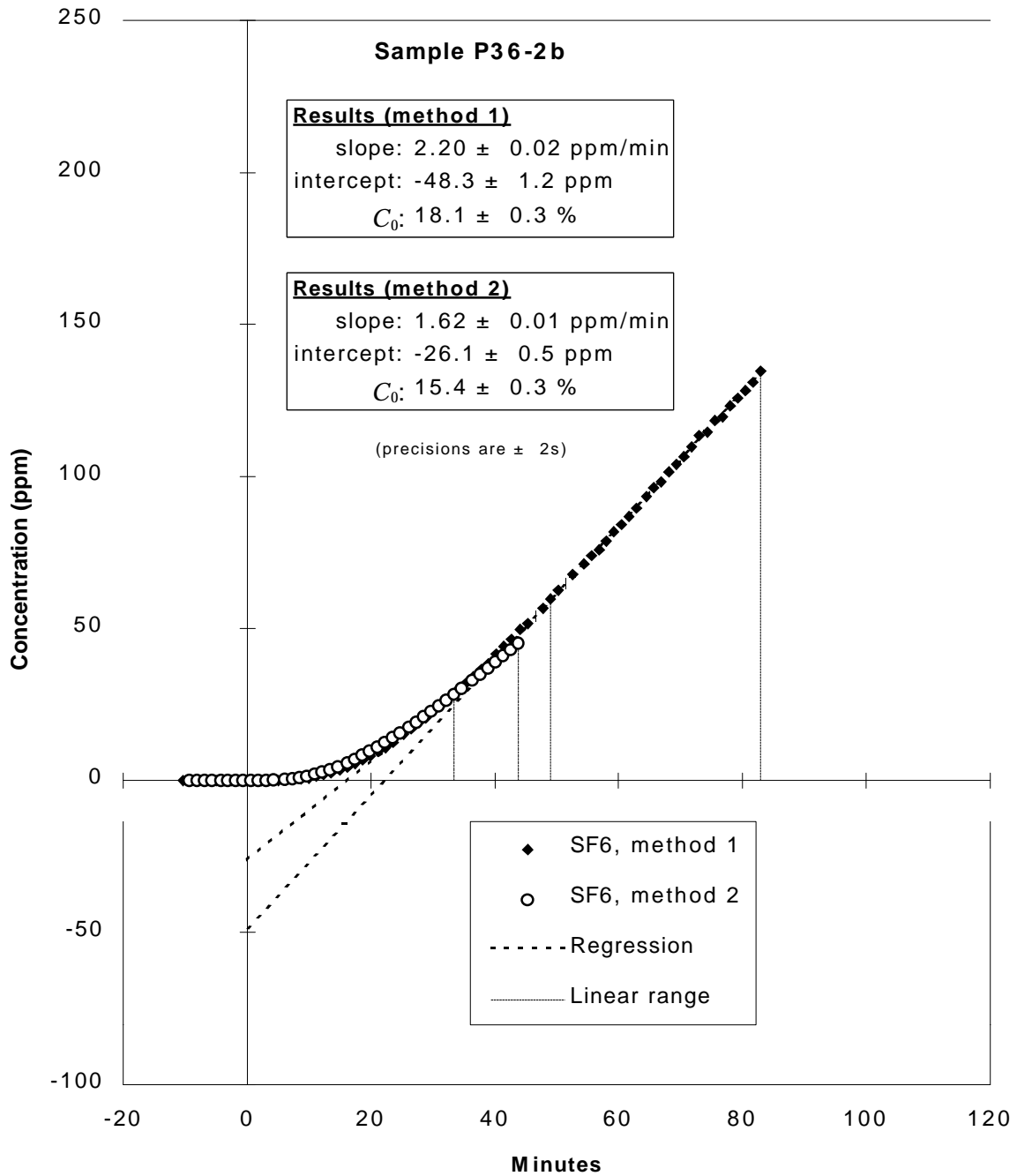$, where ρ is the density of the gas. Pure SF_6 has a specific gravity of 5.13, and the density of air at an ambient pressure of 626 torr is 0.976 kg/m^3 at $25°C$, so the density of pure SF_6 would be 5.01 kg/m^3. Thus D_0 should be 0.039 cm^2/s.

The expected value of D_0 can also be calculated from the kinetic theory of gases (cf. Atkins, 1978):

$$D_0 = \frac{1}{3}\lambda\bar{c} \text{ , where } \lambda = \frac{1}{\sqrt{2}\sigma}\frac{kT}{p} \text{ and } \bar{c} = \left(\frac{8kT}{\rho m}\right)^{\frac{1}{2}}. \qquad \{20\}$$

Here, λ is the mean free path, $\bar{c}$ is the average molecular speed, σ is the effective molecular collision cross-section (equal to ρd^2 where d is the molecular diameter), k is Boltzmann's constant, T is the absolute temperature, p is the pressure, and m is the molecular mass (146 g/mol for SF_6). The molecular diameter of SF_6 may be estimated from the radii of the constituent atoms and by assuming octahedral symmetry with the sulfur atom at the center. The molecular diameter will be approximately the sum of the diameters of two fluorine atoms and one sulfur atom, corresponding to any corner-to-corner axis through the octahedron. Possible SF_6 diameters are summarized in Table 3 for various bonding assumptions. The temperature is assumed to be 298.15 K (25.0 °C), and the pressure is taken to be 626 torr, reflecting the local air pressure in Albuquerque, New Mexico at an elevation of ~1.8 km above sea level. Converting these values to internally consistent units for use in Equation 20 gives an average speed ($\bar{c}$) of 208 m/s and a mean free path (λ) of 290–558 Å, resulting in bulk diffusion coefficients (D_0) of 0.022–0.039 cm^2/s.

The theoretical values are in good agreement with the experimentally derived value, despite the fact that the ratio of mean free path to molecular diameter is low (50–210). Both values apply to the case of self-diffusion, however, rather than diffusion into air as is the case in the present experimental work. When SF_6 is present at trace concentrations, collisions between SF_6 molecules will be rare, so diffusion will be determined by the predominant heteromolecular collisions between SF_6 and N_2 or O_2. A preliminary literature search for information on the diffusion of SF_6 into air was not fruitful, but based on the kinetic theory of gases, an argument for more rapid diffusion can be made. In air, the massive SF_6 molecules will collide more frequently with the lightweight N_2 and O_2 molecules than they would collide with other SF_6 molecules in pure SF_6, but their directions of travel will not be randomized as effectively because of their large inertia

compared to N_2 and O_2. The net result may be that the effective mean free path of SF_6 in air is greater than in pure SF_6, and hence diffusion in air would be more rapid also.

Table 3. Theoretical diffusion rates for SF_6.

Bonding	Sulfur dia. (Å)	Fluorine dia. (Å)	SF_6 dia. (Å)	D_0 (cm^2/s)
ionic	0.60	2.66	5.92	0.022
covalent	2.04	1.44	4.92	0.032
atomic	2.18	1.14	4.46	0.039

## Measured Bulk Diffusion for SF_6 Diffusion into Air

The bulk diffusion coefficient for SF_6 into air was measured using orifices of two different diameters. The larger orifice gave the highest value, of 0.073 cm/s, whereas the smaller orifice gave a value of 0.059 cm/s. Both values are larger than either the measured self-diffusion coefficient or the theoretical values derived from the kinetic theory of gases, described above. Undoubtedly part of the discrepancy is due to a mixing effect on the collection-reservoir side of the orifice related to the motion of the air as it was stirred by the fan. Mixing would tend to shorten the effective length of the orifice, causing the calculated value of D_0 to be too high. It would also have a greater effect on the larger diameter orifice because mixing could penetrate farther into the orifice due to the larger opening. Additional uncertainty is introduced by the unknown effects of variations in ambient pressure.

The present data only loosely constrain the value of D_0 for air, but suggest that it may be larger than the self-diffusion D_0 value. The larger of the two measured values (0.073 cm/s) is likely to be an upper limit, and will be used as a limiting case in the remainder of this discussion. The value of 0.039 cm/s from the self-diffusion discussion will be taken as the likely lower limit.

Expected Time-Dependent Diffusion in Portland Cement

The expected time-dependent behavior of the diffusion measurements can now be calculated given the geometry of the diffusion cell and estimated sample parameters. Results are shown in Figure 14 for a set of parameters that may resemble porous Portland cement. The porosity, f, was set to 0.30, a value typical of fine-grained materials. The tortuosity, q, was taken to be 3.00, to give profiles similar to those measured experimentally. This may be unrealistically low if this term is to be interpreted geometrically, however; Dykhuizen and Casey (1989) obtained a value for dolomite of 4.36. For a diffusion rate in air, D_0, of 0.039 cm^2/s. This calculation predicts that steady-state should be reached in ~1.5 h, and that after 4 h the concentration of SF_6 in the collection reservoir (C_C) will still be less than ~250 ppm, corresponding to a rate of increase of 1.08 ppm/min. As may be seen from Equation 8 on p. 15, the rate of increase is directly proportional to the sample diffusion coefficient (D_S), which in turn is directly proportional to the bulk diffusion coefficient (D_0) and the porosity (f), and inversely proportional to the square of the tortuosity (q) (Equation 9 on p. 15). Less obvious is the relation between these parameters and the time required to reach steady-state (t_{lin}), defined here as the time at which the linear approximation differs from the exact solution by less than 1%. Sensitivity analysis confirms the intuitive relations, showing that t_{lin}

41

increases with tortuosity (q) and decreases with bulk diffusion rate (D_0). Perhaps surprisingly, t_{lin} is not a function of porosity (f). The intercept, however, is a function of the porosity but not the tortuosity.
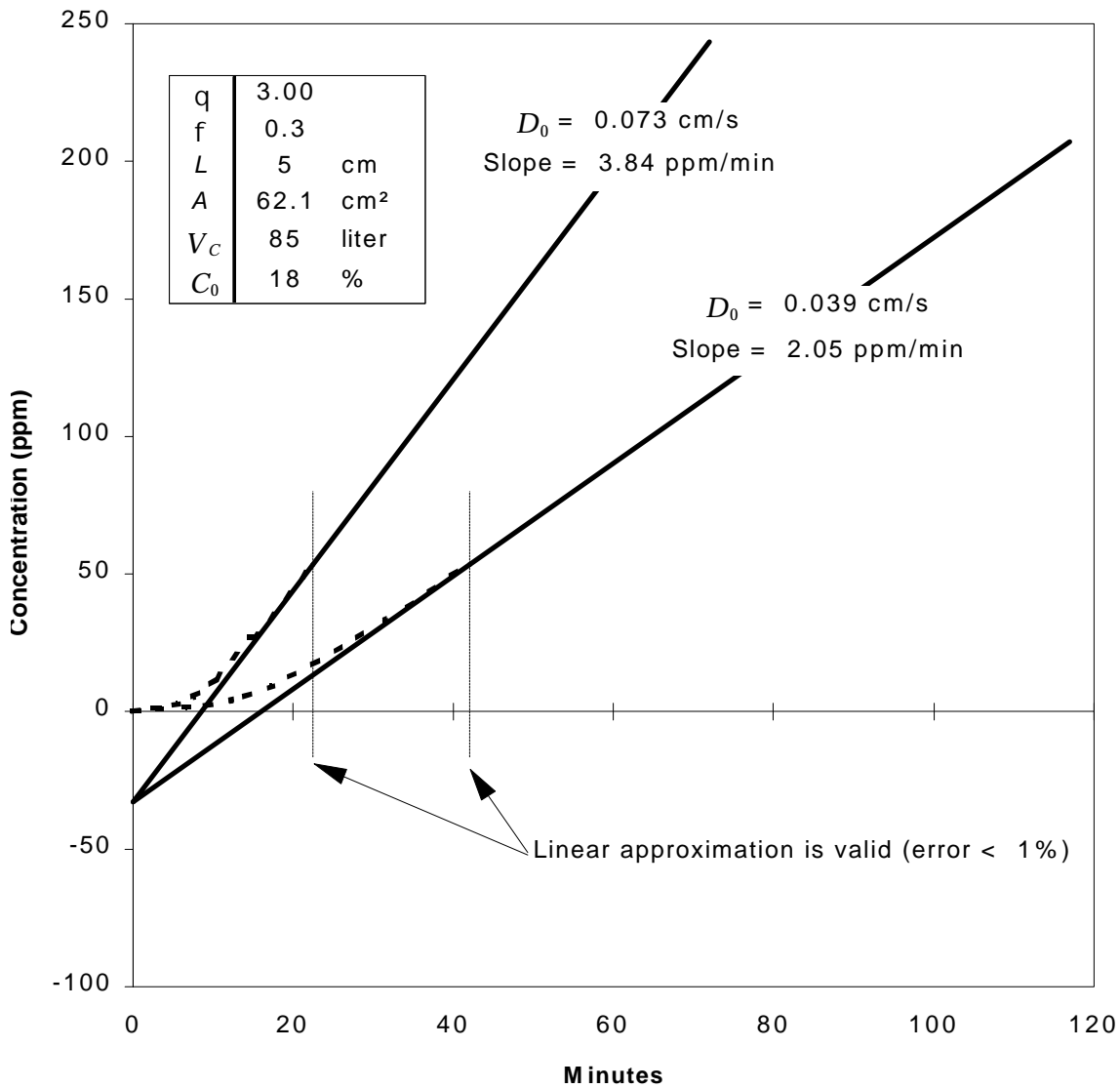
Figure 14. Expected SF$_6$ diffusion profile using likely estimates of controlling parameters.

The theoretical concentration curve versus time shown in Figure 14 suggests that steady state will be reached within 0.70 h, and that the upper concentration limit of the SF$_6$ detector (~250 ppm) will not be approached until 2 h have elapsed. Thus the collector concentration should change at a slow rate, allowing temporally accurate measurements to be made. Sensitivity analysis shows, however, that lower tortuosity (q) or a higher value for the bulk diffusion coefficient (D_0) could greatly compress this curve along the time axis to less than an hour to reach 300 ppm.

A factor that was not considered in the theoretical treatment is that SF_6 is diffusing from a region where it is present at 20% (with the balance made up of N_2) to a region containing air (21% O_2, 78% N_2, 1% Ar) where it is essentially absent. A concentration gradient similar to that driving SF_6 diffusion, but in the opposite direction, will drive diffusion of O_2 from the collection reservoir toward the SF_6 supply reservoir. The rate of diffusion of O_2 will be higher than for SF_6, perhaps by a factor of five, because of its smaller size and lower mass. Although transport of O_2 into the supply reservoir will exceed diffusion of SF_6 out of it, no pressure gradient will develop because both the supply and collection reservoirs are vented to the atmosphere. The O_2 diffusion might significantly dilute the supply gas, depending upon sample properties. If enough SF_6 diffuses through to raise its concentration in the 75-liter collection reservoir to 300 ppm, ~5 times as much O_2 may diffuse into the supply reservoir. If the supply reservoir has volume of 0.25 liters, this would correspond to a volume fraction of the supply reservoir of : 300 ppm $SF_6 \times$ 75 liters $\times$ $D_{O2}/D_{SF6}(= {\sim}5) \times 1/0.25$ liters = 45%. Clearly, however, the O_2 concentration in the SF_6 reservoir cannot exceed that in air (21%), and more likely will be only half as much (10%) or less. To correct for this, the SF_6 concentration in the supply reservoir was monitored at the end of each run to assess the extent of dilution.

Experimental Measurements and Derived Parameters

The raw experimental data of slope and intercept provides the necessary inputs for calculating transport parameters, as listed in Table 5. Constants used in the calculations are given in Table 4. The effective diffusion coefficient (D_S) for each sample was calculated using Equation 8 (p.15). It depends only on the slope, the supply reservoir concentration (C_0) and the physical dimensions of the sample and diffusion cell; it is the proportionality constant relating flux to concentration gradient. The porosity (f) is similarly fundamental, depending only on the intercept and on C_0 and the physical dimensions. It was calculated using Equation 12 on p.16. At a greater level of abstraction is the tortuosity (q, the ratio of the actual average path length to the sample length), which is derived from D_S, f, and the bulk diffusion coefficient (D_0) according to Equation 9 on p.15.

The diffusive properties are related to fluid flows due to differences in piezometric head by the *Kozeny-Carman equation* (Equation 16 on p.17) for permeability (k) and the general equation for hydraulic conductivity (K, Equation 14 on p.17). The *Kozeny-Carman equation* provides an empirical relation between f and k, and also requires an estimate of the specific surface area and the density of the matrix. The matrix density of Portland cement was taken to be the average of portlandite ($r = 2.24$ g/cm^3) and quartz (a representative soil mineral, with $r = 2.65$ g/cm^3), giving a value of 2.45 g/cm^3 for r_m. Equation 14 on p.17 relates K to k and the fluid's density and dynamic viscosity, given in Table 4 for pure water at 25°C.

The effective diffusion coefficients appear to be significantly different between the two groutings that were sampled. Both experimental methods gave similar results for D_S, averaging 0.0028 for P36-1 and 0.0011 for P36-2, values over an order of magnitude less than for SF_6 diffusion in air (D_0). Method 1, with continuous SF_6 flow, yielded slightly higher D_S values for all four samples, due either to the presence of a slight pressure differential in this method, or to inaccurate

estimates of C_0 in method 2. The combined results for both methods suggest an accuracy for these measurements of ~10% (1S), with slightly better precision for each method individually. Interestingly, D_S is anti-correlated with macroscopic texture and is unrelated to the presence of hairline cracks. Grouting P36-1 has fewer voids than P36-2 but higher D_S. No difference in D_S was observed between P36-1a and P36-1b, although P36-1b contains numerous hairline fractures. Additionally, no difference was observed between P36-2a and P36-2b even though P36-2b contains a large fracture that was filled with epoxy during sample preparation. These results also suggest that differences in sample preparation did not produce measurable effects.

Table 4. Constants used in calculations.

Parameter	Value	Units
V_C	84.88	liters
r_m	2.45	g/cm³
r	0.997	g/cm³
g	980	cm/s²
m	0.0089	g/cm·s

Table 5. Measurements and derived parameters.

Sample	C_0	slope	intercept	D_S	f	q^1	q^2	log k	K
	(%)	(ppm/min)	(ppm)	(cm²/s)	(cm³/cm³)	(cm/cm)		(cm²)	(cm/s)
Method 1									
P36-1a	17.9	5.26	-65.15	0.0030	0.52	2.4	3.5	-6.7	0.0227
P36-1b	18.2	5.21	-63.85	0.0030	0.50	2.4	3.5	-6.8	0.0186
P36-2a	18.2	2.68	-66.32	0.0014	0.55	3.6	5.3	-6.5	0.0325
P36-2b	18.1	2.20	-48.35	0.0011	0.42	3.6	5.2	-7.1	0.0097
Method 2									
P36-1a	13.7	3.77	-38.86	0.0026	0.45	2.6	3.6	-6.9	0.0126
P36-1b	14.9	3.86	-32.98	0.0027	0.32	2.2	3.0	-7.7	0.0022
P36-2a	10.4	1.06	-24.90	0.0010	0.36	3.8	5.2	-7.4	0.0045
P36-2b	15.4	1.62	-26.09	0.0010	0.27	3.3	4.5	-7.9	0.0015

[1] Calculated assuming $D_0 = 0.034$ cm²/s.

[2] Calculated assuming $D_0 = 0.073$ cm²/s.

The apparent porosity values lack the systematic trends observed in the calculated diffusion coefficients, with variations from method 1 to method 2 of ~40% for the same sample, and variations between samples from the same grouting of up to ~25% for the same method. The actual f values are not known, but are probably unlikely to exceed 0.25–0.30. Allan and Kukacka (1995) report an average bulk density for other samples from the same grouting array of 2.006 g/cm³, which would correspond to a porosity of 0.18 if a matrix density of 2.45 g/cm³ is assumed.

Several factors may have contributed to these scattered and seemingly large porosity values, such as an inaccurate estimate of the time required to fill the supply reservoir before diffusion can be said to begin, variation of D_0 as a function of its concentration in air, and decreases in the ambient pressure causing unaccounted-for delays in the attainment of steady-state. All of these factors could affect the value of the intercept at $t = 0$. For lack of better estimates of f, however, these values will be used in the subsequent analysis for q, k, and K.

Surprisingly, the tortuosity shows greater consistency than the porosity, in part because it is related to the square root of the porosity (and D_0, and $1/D_S$). Tortuosities were calculated for limiting values of D_0 (0.034 and 0.073 cm/s). Use of the higher value led to q values of 3.0–5.3, bracketing the value observed by Dykhuisen and Casey (1989) of 4.36. The following discussion uses the higher D_0 value. Both method 1 and method 2 indicate that grouting P36-1 has a lower tortuosity (~3.4) than P36-2 (~4.9). Further work is needed to determine the extent to which these tortuosities have physical significance. It is suggestive, however, that the grouting with low D_S has high q.

Calculated permeabilities are near 10^{-7} cm^2, giving rise to calculated conductivities near 10^{-2} cm/s for all four samples. Method 1 gave somewhat greater values due to the greater porosities discussed previously. These conductivities are much higher than those reported by Allan and Kukacka (1995) for other samples from the same grouting array, which were in the range 10^{-8}–10^{-9} cm/s. Allan and Kukacka made their measurements under saturated aqueous conditions, however, where the cement gel in these groutings would have swelled significantly (Lea, 1971). This would have reduced porosity and drastically constricted the throats between adjoining pores, thereby greatly reducing permeability and hydraulic conductivity. Thus, gas permeability is expected to be much greater than aqueous permeability for cement-based materials, but this may not be responsible for the entire six-order-of-magnitude difference. Recall that the *Kozeny-Carman equation*, used to related porosity and specific surface area to conductivity, was calibrated empirically for granular media, so some degree of inaccuracy is to be expected when applying it to a porous gel such as cement. Resolution of this issue will require further intercomparisons of gas-diffusion versus saturated aqueous methods, including measurements on samples of stable geometry (i.e., non-swelling in the presence of water).

Feasibility of Field-Scale Measurements

Gas diffusion measurements show promise as a tool for studying the integrity on barriers in field settings, in addition to evaluating *ex situ* prepared samples in the laboratory. Diffusion of SF$_6$ through grout (a mixture of soil and cement) is at least an order of magnitude slower than diffusion through air, so the method should be sensitive to the presence of open fractures, large voids, or other discontinuities in the grout. Nevertheless, diffusion of SF$_6$ through grout is rapid enough so that measurements will require a matter of days rather than months or years. The time required to reach steady state is proportional to the square of the length over which diffusion is to be measured (cf. Equation 11 on p.16), so extrapolating from the laboratory where ~20 min was required to reach steady-state for a 5 cm length to a distance of 1 m in the field suggests that ~5.6 days would be required. The principle difficulty may be to minimize alternate flow paths between source and detector, either through the soil or the ambient atmosphere rather than the barrier.

Gas diffusion presents an important advantage relative to aqueous tracer studies under field conditions to verify the integrity of a barrier: it is essentially non-destructive. In one conceptualization, a small hole could be bored to the center of the barrier for the introduction of SF_6, and an array of sniffers could be located around the outside of the barrier. (The sniffers would be multiplexed to a single gas analyzer and would be sampled sequentially.) Gas could be introduced at atmospheric pressure to ensure only diffusional transport, or at slightly elevated pressure to speed up the approach to steady state and increase the flux to the sniffers. Integrity would be assessed by comparing observed profiles of concentration versus time with predictions based on the barrier geometry. Empirical assessment might also be possible by taking advantage of any symmetry in the barrier geometry and comparing equivalent flow paths.

Summary

This study shows that it is practical to measure SF_6 diffusion rates in the laboratory on samples of grout (Portland cement and soil) typical of what might be used in a barrier. This study has demonstrated the following points at the laboratory scale:

- SF_6 is a nearly ideal tracer — inert with respect to most materials and readily detectable at trace levels (down to 5 ppb).

- Diffusion of SF_6 into air may be as rapid as 0.073 cm^2/s, based on direct measurement, which is higher than self-diffusion or theoretical predictions.

- Diffusion of SF_6 through desert soil grouted with Portland cement is on the order of 0.001–0.003 cm^2/s.

- Measurement times for laboratory samples (9.5 cm dia. $\times$ 5 cm long) are less than 1 h.

- Measurements of D_S are reproducible to $\pm$ 10% or better, and show a factor-of-two variation between two groutings while showing little variation among duplicates of the same grouting.

- Calculated values for porosity are high and scattered, suggesting incomplete understanding of possible experimental influences.

- Tortuosity values, based in part on porosities, are anti-correlated with D_S, and thus may have physical significance.

- Direct comparisons of gas-diffusion versus saturated aqueous methods are needed on samples of stable geometry (i.e., non-swelling in the presence of water) in order to understand the relationship between gas diffusion and hydraulic conductivity in a cement matrix.

These results suggest that field-scale tests would also be feasible, and would provide a non-destructive method of evaluating the integrity of a barrier *in situ*. Field-scale measurements should be practical on time-scales of a few days, and diffusion of SF_6 through air is at least an order of magnitude faster than through cement, so fractures should be readily detectable, if present.

Intentionally Left Blank

References

Allan, M.L. and L.E. Kukacka, 1994: *In-Situ Containment and Stabilization of Buried Waste.* Fiscal year 1994 Annual Report BNL-60977, Brookhaven National Laboratory, Upton, New York.

Allan, M.L. and L.E. Kukacka, 1995: *Analysis of Core Samples from Jet Grouted Soil.* Informal Report BNL-62357, Brookhaven National Laboratory, Upton, New York, 13 p.

Atkins, P.W., 1978: *Physical Chemistry.* W.H. Freeman and Co., San Francisco, California, 1018 p.

Bear, J., 1972: *Dynamics of Fluids in Porous Media.* Dover Publications, Inc., New York, 764 p.

Carslaw, H.S. and J.C. Jaeger, 1959: *Conduction of Heat in Solids, Second Edition.* Oxford University Press, New York, 510 p.

Dykhuizen, R.C. and W.H. Casey, 1989: An Analysis of Solute Diffusion in Rocks. *Geochimica et Cosmochimica Acta*, v. 53, p. 2797–2805.

Franz, E.-M., M. Fuhrmann, B. Bowerman, S. Bates, and R. Peters, 1994: Proposed Waste Form Performance Criteria and Testing Methods for Low-Level Mixed Waste. *Brookhaven National Laboratory Formal Report*, BNL-52436 or DOE/MWIP-30, 153 p.

Heiser, J. and B. Dwyer, 1995: *Demonstration of Close-Coupled Barriers for Subsurface Containment of Buried Waste*. Informal Report BNL-62573, Brookhaven National Laboratory, Upton, New York, 65 p.

Lea, F.M., 1971: *The Chemistry of Cement and Concrete.* Chemical Publishing Co., New York, 727 p.

Stefanov, B., L. Zarkova, L.R. Folkin, V.E. Lyusternik, V.V. Altunin, and E.E. Tozkii, 1991: Thermophysical Properties of Gaseous Sulphur Hexafluoride in the Range 220–1000 K: 43 Experiments Described by a Unique Intermolecular Potential. *High Temperatures-High Pressures*, v. 23, p. 461–471.

Weast, R.C., 1973: *Handbook of Chemistry and Physics*. CRC Press, Inc., Cleveland, OH.

Distribution

3   U.S. Department of Energy
Attn: Skip Chamberlain
EM-54, Cloverleaf Center
19901 Germantown Rd.
Germantown, MD 20874-12901

1   U.S. Department of Energy
Attn: Caroline Purdy
EM-53, Cloverleaf Center
19901 Germantown Rd.
Germantown, MD 20874-12901

1   U. S. Department of Energy
Savannah River Operations Office
Attn: Scott McMullin
Building 703-46A
P.O. Box A
Aiken, SC 29802

1   U. S. Department of Energy
Savannah River Operations Office
Environmental Sciences Section
Attn: Mike Serrato
P.O. Box 616 / 773-42A
Aiken, SC 29802

1   U. S. Department of Energy
Albuquerque Operations Office, ETN
Attn: Dennis Olona
Pennsylvania/H Street
Albuquerque, NM 87116

1   Brookhanven National Laboratoy
Attn: John Heiser
34 North Railroad Ave.
Building 830
Upton, NY 11973

1   Science & Engineering Associates, Inc.
Attn: Sandy Dalvit Dunn
1570 Pacheco, Suite D-1
Santa Fe, NM 87501

1   Thomas Branigan Library
Attn: D. Dresp
106 W. Hadley St.
Las Cruces, NM 88003

1   Government Publications Department
Zimmerman Library
University of New Mexico
Albuquerque, NM 87131

3	MS0706	C.V. Williams, 6113
1	0719	G. C. Allen, 6621
1	0719	J. D. Betsill, 6621
5	0719	T. D. Burford, 6621
1	9018	Central Technical Files, 8940-2
5	0899	Technical Library, 4916
2	0619	Review & Approval Desk, 12690 for DOE/OSTI

50